

## Chapter 2

# Overview of LiDAR Technologies and Equipment for Land Cover Scanning

**Abstract** The land cover of the Earth's surface impacts strongly on the climate and environment. Precise monitoring of land cover plays the significant role in the management of the natural resources and planning humanity development. In this sense, a remote sensing is an indispensable tool for study and prediction the global, regional, and local ecological issues. A remote sensing implies the use of satellite, airborne, and terrestrial shootings or their combination. In this book, the airborne and terrestrial shootings are discussed as the factors that contribute greatly in the study of the natural resources. Both types of shooting are based on the laser scanning of areas, using the LiDAR technologies. The terrestrial shooting is executed by the stationary (with a tripod use) and mobile laser scanning systems (using the cars, trams, or ships). At last decades, the laser scanning based on the Unmanned Aerial Vehicles (UAVs) started to be applied. In this chapter, an overview of the LiDAR techniques and equipment for the different types of laser scanning is given.

**Keywords** LiDAR technologies • Airborne laser scanning • UAV-based scanning • Terrestrial laser scanning • Mobile laser scanning • Hand-held laser scanning

## 2.1 Introduction

The remote sensing is an efficient tool to acquire the forest monitoring in global, regional, and local scales. The airborne LiDAR systems that emerged commercially in the middle of 1990s, provide the explicit 3D laser profiling and scanning in contrast to the 2D planimetric remote sensing data. The 3D coordinates ( $x$ ,  $y$ ,  $z$ ) of a point cloud describe the 3D topographic profile of the Earth's surface, vegetation cover, and man-made objects. The airborne LiDAR technique has been effectively used for generating the Digital Elevation Model (DEM), the Digital Terrain Model (DTM), and the Digital Surface Model (DSM). On the one hand, an airborne shooting does not

sensitive to the lighting conditions. On the other hand, the meteorological conditions, as the cloudy or foggy days, influence negatively on the shooting results.

In 1999, Ackermann [1] pointed out three directions of airborne laser scanning, such as the extended applications, the consolidation and extension of the LiDAR data processing methods, and the additional information about the Earth's surface characteristics. Further, these propositions were proved in academic and industrial spheres. The outstanding review about laser scanners and their features, classification techniques, and further development of the LiDAR data processing was provided by Yan et al. [2].

Usually the Airborne Laser Scanning (ALS) and the Terrestrial Laser Scanning (TLS) systems record the indirect signal intensity that causes the problems in comparison to the use of the direct recorded values. The transmission loss and the topographic and atmospheric effects influence on the backscatter of the emitted laser power. This leads to a noticeably heterogeneous representation of the received power. The geometric and radiometric calibrations help to solve this problem.

The active remote sensing technique delivers not only detailed information about the coordinates but also data about the reflectance characteristics of the Earth's surface in the laser wavelength. Typically, the ALS systems provide the signal in the Near-Infrared (NIR) spectra in the wavelength interval 800–1550 nm. The ALS systems record the return amplitude of echoes with a full-waveform digitization. The emitted laser shot interacts with the surface, generating the backscatter. The received signal as a function of time contains one or more peaks that correspond to the distinct reflections of a laser beam from the opaque or penetrable (like trees or shrubs) objects. Notice that in a field of the ALS, the terms “signal intensity”, “reflectance intensity”, and “pulse reflectance” are often used as synonym for the return amplitude or energy of one echo. As Höfle and Pfeifer mentioned in [3], the ALS systems, recording the intensity, are the small footprint scanners that operate with a beam divergence in the range of 0.3–0.8 mrad and a flying altitude above ground up to 3500 m. Herewith, the laser footprint diameter (with a beam divergence of 0.8 mrad) would be 0.8 and 2.8 m for the flying heights of 1000 and 3500 m, respectively. The spatial resolution (a footprint area) for cameras may vary strongly that caused by the changes in the flying altitude and the topography of the scanned surface (under the assumption that a beam divergence is constant during a flight). The variations in scan geometry lead to the appearance of the under-sampling (gaps) and over-sampling (overlapping footprints) that requires a re-computation of the obtained signal according to topography and flying altitude.

The chapter is organized as follows. The development of the LiDAR technologies is discussed in Sect. 2.2. An overview of airborne, the UAV, and terrestrial laser scanning, including the basic physical principals, methods of registration, and equipment, is represented in Sects. 2.3–2.5, respectively. In spite of the UAV laser scanning is a type of the ALS, it is reasonable to discuss it in separate section because of the principal differences in navigation and equipment. Section 2.6 includes a comparison of remote sensing techniques for forest inventory. Conclusions are drawn in Sect. 2.7.

## 2.2 Development of LiDAR Technology

Periodically, the global airborne LIDAR market reports are becoming available at internet sites. Thus, Cary and Associates of Longmont, CO. [4] analyzed the global airborne LIDAR market from 2005 to 2008. The survey indicated that there has been an increase of 64% in the number of LiDAR systems in use, 53% in LiDAR operators, and 100% in the number of end-users in that period. Looking out to 2012, the report predicted that the sales of software and data processing services will grow from 11 to 20% range. A list of the LiDAR applications included:

- Topographic mapping [5–9].
- Flood risk assessments [10–13].
- Watershed analysis [14].
- Forestry modeling and analysis [8, 15–25].
- Habitat ecology [26–28].
- Landslide investigation [29].
- 3D building modelling [30–32].
- Road extraction [33].
- Snow depth measurement [34].

At last decades, various methods (such as LiDAR data filtering, the DTM/DEM/DSM generation, full-waveform data modelling, geometric and radiometric calibration, among others) and data formats of LiDAR data processing were developed. The American Society of Photogrammetry and Remote Sensing (APSRs) also provided a platform for the formulation of the Log ASCII Standard (LAS) data format from version 1.1–1.4 [35–39] with the guidelines and manual for manipulating of the airborne LiDAR data. Besides, the International Society for Photogrammetry and Remote Sensing (ISPRS) had offered three benchmark testing datasets for examining the algorithms and methods for urban object classification and 3D building reconstruction [32]. Also the ISPRS international conferences are organized.

The commercial topographic LiDAR sensors usually utilize the near-infrared laser with the wavelength 1064–1550 nm. The returned signal is characterized by a high separability of spectral reflectance that permits to separate different land cover materials. As a result, a continuous high resolution 1D waveform profile can be built [40, 41]. Table 2.1 provides some studies that demonstrate the use of airborne LiDAR for land cover classification in terms of the scanning configuration, data resolution, a number of feature spaces used, classification technique, and overall accuracy in 2004–2012 (some data were taken from [2] and checked using the initial references).

In report [55], the state of LiDAR market is forecasted from 2016 to 2022. The LiDAR market was studied in 2015 and valued at USD 1.39 Billion in 2016. It is expected to reach USD 3.22 Billion by 2022, at the Compound Annual Growth Rate (CAGR) of 12.4% from 2016 to 2022. It was found that the terrestrial lasers hold the largest share of the LiDAR market among all product types. Key companies,

**Table 2.1** List of studies using airborne LiDAR for land cover classification

Case study	Laser scanning configuration	Data resolution	Feature spaces	Classification technique	Overall accuracy (%)
Charaniya et al. [42]	PR = 25 kHz; PS = 0.26 m; WL = 1064 nm	0.5 m	2–5	4 classes. Gaussian mixture models	66–84
Brennan and Webster [43]	BD = 0.45 mrad, FH = 950 m, PR = 40 kHz, SR = 17 Hz, WL = 1064 nm	1 m	5	7–10 classes. Object-oriented	94–98
Lodha et al. [44]	PR = 25 kHz, PS = 0.26 m, WL = 1064 nm	0.5 m	5	3–4 classes. Support vector machine	89–96
Farid et al. [45]	ALTM 1233. FH = 750 m, FP = 15 cm, SR = 28 Hz, SA = $\pm 20^\circ$ , WL = 1064 nm	0.9 m	4	7 classes. Maximum likelihood	78–80
Lodha et al. [46]	PR = 25 kHz, PS = 0.26 m, WL = 1064 nm	0.5 m	5	4 classes. AdaBoost	92–96
Orka et al. [47]	Optech ALTM 3100. BD = 0.26 mrad, FH = 7500 m, FS = 75 m/s, FP = 264 m, PR = 100 kHz, SR = 70 Hz, SA = $\pm 10^\circ$ , PD = 5.09 pts/m <sup>2</sup>	0.21 m	4	3 classes. Linear discriminant analysis	68–74
Im et al. [48]	Optech ALTM 2050 LiDAR OptechALTM 2050 LiDAR PD = 15.3 pts/m <sup>2</sup> , PR = 50 kHz, PS = 0.4 m, WL = 1064 nm	0.25 m	8	5 classes. Object-based, decision trees	92–94
Goncalves et al. [49]	Optech's ALTM 2033 ( <a href="http://www.optech.ca">www.optech.ca</a> ). BD = 0.3 mrad, FH = 1500 m, PR = 33 kHz, SR = 50 Hz, SA = $\pm 10^\circ$ , WL = 1064 nm, PD = 4 pts/m <sup>2</sup>	0.5 m	3	4 classes. Maximum likelihood, hierarchical classification, object-oriented	85–92
Kim et al. [50]	Optech ALTM30/70. BD = 0.31 mrad, FH = 1200 m, SA < $110^\circ$ , PR = 71 kHz, PD = 5 pts/m <sup>2</sup> , WL = 1064 nm and Optech ALTM 3100. BD = 0.31 mrad, PR = 100 kHz, SA < 10, PD = 20 pts/m <sup>2</sup> , WL = 1064 nm. For both systems FP = 0.372 m with leaf-on data and FP = 0.279 m with leaf-off data	0.21 m	5	15 classes. Linear discriminant analysis	83–91

(continued)

Table 2.1 (continued)

Case study	Laser scanning configuration	Data resolution	Feature spaces	Classification technique	Overall accuracy (%)
Habib et al. [51]	Leica ALS50, BD = 0.330 mrad, FH = 600 m, PR = 83 kHz, PD = 4–5 pts/m <sup>2</sup> , WL = 1064 nm	0.2 m	1–2	3–5 classes. Maximum likelihood	30–70
Yan et al. [52]	Leica ALS50, BD = 0.33 0mrad, FH = 600 m, PR = 83 kHz, PD = 4–5 pts/m <sup>2</sup> , WL = 1064 nm	0.2 m	1–2	5 classes. Geometric and radiometric corrections	43–70
Buján et al. [53]	Optech ALTM 3025, BD = 0.2 mrad, FH = 1300 m, PR = 25 kHz, PD = 4 pts/m <sup>2</sup>	0.5 m	5	6 classes. Object-based, decision trees	93–97
Shaker and El-Ashmawy [54]	Leica ALS50 BD = 0.33 mrad, FH = 600 m, WL = 1064 nm	0.2 m	4	4 classes. Principle component analysis	70–73

*BD* is a beam divergence, *FH* is a flying height, *FP* is a footprint, *FS* is a flying speed, *PD* is a point density, *PR* is a pulse rate, *PS* is a point spacing, *SR* is a scan rate, *SA* is a swath (scan) angle, *WL* is a wavelength

operating in the market, are the Quantum Spatial (Aerometric) (U.S.), the Faro Technology (U.S.), the Geodigital (Canada), the Leica Geosystems AG (Switzerland), the Optech, Inc. (Canada), the Riegl Laser Measurement Systems GmbH (Austria), the Topcon Positioning Systems, Inc. (U.S.), the Trimble Navigation Limited (U.S.), the Sick AG (Germany), the Velodyne (U.S.), the BLOM (Norway), the Michael Baker International (U.S.), and the YellowScan (France).

## 2.3 Overview of Airborne Laser Scanning

A typical LiDAR system consists of a laser scanner and Global Positioning System/Inertial Navigation System (GPS/INS) navigation components. The laser scanner mounted on the platform produces a wide swath over, which the distances to the mapped surface are measured. The distances from the sensor to the mapped surface are computed by the time delay between the laser pulse transmission and detection. The laser beam direction (an encoder angle), at which the laser is scanned, is measured. The onboard GPS/INS components provide the position and orientation of the platform's movement. Then all types of information are used in the post-processing in order to calculate the coordinates of the point cloud. The laser technology was invented by Charles Townes and Arthur Schawlow in Bell Labs in 1958. Since that time, many investigations were done that was reflected in numerous publications, e.g., the books [56–58].

The physical principles of airborne laser scanning are discussed in Sect. 2.3.1. Section 2.3.2 explains the sources of the main errors, appearing during a laser scanning. Sections 2.3.3–2.3.4 provide the conventional and alternative LiDAR calibration methods, respectively. An overview of the equipment for airborne laser scanning is represented in Sect. 2.3.5.

### 2.3.1 Physical Principles of Airborne Laser Scanning

The basic measuring principle of laser scanning (airborne, using the UAV, or terrestrial) is the same but with the own features of application. Jelalian [59] proposed the radar range equation under the assumption that the receiver field of view matches the beam divergence and emitter and detector have the same distance to the target. Equation 2.1 comprises the sensor, target, and atmospheric parameters, where  $P_r$  is a received signal power,  $P_t$  is a transmitted signal power,  $D_r$  is a receiver aperture diameter,  $R$  is a range from sensor to target,  $\beta_t$  is a laser beam width,  $\eta_{sys}$  is a system transmission factor,  $\eta_{atm}$  is an atmospheric transmission factor,  $\sigma$  is a target cross-section.

$$P_r = \frac{P_t D_r^2}{4\pi R^4 \beta_t^2} \eta_{\text{sys}} \eta_{\text{atm}} \sigma \quad (2.1)$$

The effective target cross-section (backscattering cross-section)  $\sigma$  contains all target characteristics and is defined by Eq. 2.2, where  $\Omega$  is s scattering solid angle of the target,  $\rho$  is a target reflectance,  $A_s$  is a target area.

$$\sigma = \frac{4\pi}{\Omega} \rho A_s \quad (2.2)$$

The direction of the reflection is determined by the angle of incidence  $\alpha$ . This is an angle between the laser beam and the target area. It is defined as an angle enclosed by a surface normal and a laser shot direction. The reflectance is an averaged over the total target area portion of reflected to incident radiation from the target area in the laser wavelength. The specular or diffuse reflections influence differently on the direction and strength of the backscattering cross-section. The target size is the effective area illuminated by the laser beam, i.e., the size of the orthogonal-to-ray projected area of the scatterer.

Jelalian [59] introduced the simplification of Eq. 2.2 under the following assumptions:

- The entire footprint is reflected on one surface (extended target) and the target area  $A_s$  is circular. Hence, the entire footprint is defined by the laser beam width  $\beta_t$  and the range  $R$ .
- The target has a solid angle of  $\pi$  steradians ( $\Omega = 2\pi$  for scattering into a half sphere).
- The surface has the Lambertian scattering characteristics. If an incident angle is greater than zero ( $\alpha > 0^\circ$ ), then a target cross-section  $\sigma$  has a proportionality of  $\cos \alpha$  [60, 61].

As a result, the parameters  $A_s$  and  $\sigma$  can be calculated, using Eqs. 2.3–2.4.

$$A_s = \frac{\pi R^2 \beta_t^2}{4} \quad (2.3)$$

$$\sigma = \pi \rho R^2 \beta_t^2 \cos \alpha \quad (2.4)$$

A substitution of Eqs. 2.3–2.4 in Eq. 2.1 leads to an inverse range square dependency of the received signal power, independent of the laser beam width (Eq. 2.5).

$$P_r = \frac{P_t D_r^2 \rho}{4R^2} \eta_{\text{sys}} \eta_{\text{atm}} \cos \alpha \quad (2.5)$$

Jelalian [59] show that the areas of the non-extended diffuse targets have different range dependencies. Thus, the point targets with an area smaller than the

footprint (e.g., a leaf) are range independent. The linear targets areas (e.g., a wire) are linear range dependent. As a consequence, the received power reflected from the non-extended targets underlies an inverse range-dependent function with higher power ( $1/R^4$ ,  $1/R^3$ ). Often the ALS systems do not record the emitted power or even the emitted waveform. Hence, the optical transmission efficiency of all optical components in the ALS system as well as the system transmission factor  $\eta_{\text{sys}}$  are assumed to be constant for a certain ALS system but vary for different systems and over time. The aperture diameter  $D$  is also set to be a constant factor.

The system-independent atmospheric effect defined by  $\eta_{\text{atm}}$  stands for the average atmospheric conditions at the time of a flight. A wavelength range strongly influences on the loss of energy primarily due to scattering and absorption of the laser photons in the atmosphere between the scanner and target, even if the atmospheric conditions are constant. For a wavelength of 1.06  $\mu\text{m}$ , the effect of scattering considerably exceeds a contribution of absorption [62]. For horizontal propagation, the attenuation  $a$  can range from 0.2 dB/km for extremely clear conditions to 3.9 dB/km for haze conditions [59]. For vertical propagation, the atmospheric transmittance typically increases with higher altitudes (the vertical propagation results in lower average attenuation coefficients in comparison to the horizontal propagation). For flying heights of 1000, 2000, and 3000 m above ground and above sea level, the average vertical attenuations are 0.22, 0.17, and 0.14 dB/km, respectively (these values were obtained for mid-latitude summer and rural aerosol conditions with a visibility of 25 km). Equation 2.6 helps to evaluate an influence of the atmospheric factors, where  $a$  is an atmospheric attenuation coefficient, dB/km,  $R$  is a range from sensor to target, m, the factor 10,000 originates from a given in dB per km.

$$\eta_{\text{atm}} = 10^{-2Ra/10000} \quad (2.6)$$

From practical experience, the noise in the intensity measurement is around 10%. On the one hand, a value of the atmospheric transmission factor  $\eta_{\text{atm}}$  can be neglected due to very clear atmospheric conditions and small ranges. On the other hand, the model covers the large range differences. This leads to consider the factor  $\eta_{\text{atm}}$ . Due to the lack of meteorological data (e.g., temperature, water vapor, or aerosol concentration) and the high spatial variability of these parameters, an approximated value for parameter  $a$  has to be chosen as the average atmospheric conditions of a flight. Equation 2.5 can be rewritten, where factor  $C$  represents the sensor parameters (e.g.,  $P_r$ ,  $D$ , system losses) that are assumed to be constant within a flight, using the same ALS system settings.

$$P_r(R) = \alpha \frac{P}{R^2} 10^{-Ra/10000} \cos \alpha \cdot C \quad (2.7)$$

The left side of Eq. 2.7 is converted into a voltage, amplified in the ALS system, and finally transformed into a digital form through an unknown proprietary function. Assuming a linearity in this transformation, it is further possible to compare



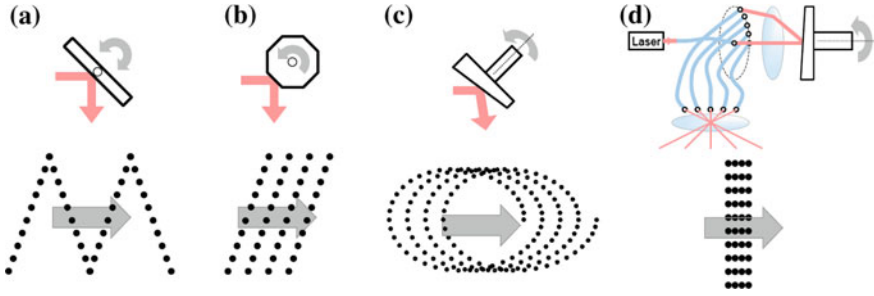


**Fig. 2.1** Scanning mechanisms and ground patterns: **a** oscillating mirror and linear pattern (Z-shaped), **b** rotating polygon and linear pattern (parallel), **c** nutating mirror (palmer scan) and elliptical pattern, **d** fiber switch and linear pattern (along the *flight lines*)

the intensity measurements. The peaks of the Gaussian pulse waveforms can be compared (not more than 50% of a range width). Having the target areas with a defined reflectance  $\rho$  measured by a spectrometer on the ground, one can estimate a direct determination of parameter  $C$ . The normalization of the intensity to an average range and the estimation of  $C$  offer a reasonable approximation of surface reflectance under the mentioned above assumptions.

The LiDAR scanning pattern on the ground is affected by the scanning device, as well as the flight path, the flight speed, and the terrain topography. The types of scanning devices used in the commercial LiDAR systems are the following: an oscillating mirror, a rotating polygon, a nutating mirror, and a fiber switch. Their schematic illustrations are depicted in Fig. 2.1.

The oscillating mirror and rotating polygon yield the linear scanning patterns: the “zigzag” patterns (Fig. 2.1a) and the parallel lines on the ground (Fig. 2.1b), respectively. The non-linear scanning pattern is produced by the nutating mirror, providing an elliptical path of the laser beam (Fig. 2.1c). The advantage of the nutating mirror is that the ground is scanned twice from different directions (forward and backward). This means that the occluded areas in the forward scanning can be captured in the backward scanning. The fiber scanner consists of two arrays of glass fibers, transmitting and receiving. The number of glass fibers determines the number of laser footprints across the flying direction (Fig. 2.1d). The fiber scanner has an important advantage with respect to maintaining the stability of measuring laser beam directions because each glass fiber has a fixed beam direction. According to the reviews of the commercial LiDAR systems [63], the oscillating mirror and rotating polygon are the most popular.

The coordinates of the LiDAR footprints are the result of combining the derived measurements from each of its system components as well as the boresight and lever-arm parameters relating to such components. The relationship between the system measurements and the parameters is embodied in the LiDAR georeferencing equation [64], considering four coordinate systems, such as a mapping frame (ground coordinate system), an Inertial Measurement Unit (IMU) body frame, a laser unit frame, and a laser beam frame.

### 2.3.2 Errors of LiDAR Systems

The random and systematic errors are the main types of errors in the LiDAR system. The random errors are the errors of the system's measurements (the position and orientation of the integrated GPS/INS, encoder angles, and laser ranges) and provide a frequency distribution, usually normal distribution. The systematic errors are caused by the physical laws, can be predicted, and may lead to the biases in the boresight angles and lever-arm offsets of the system components and biases in the encoder angles and laser ranges of the system measurements.

The impact of random errors on the obtained point cloud can be studied by two ways. The first approach is based on a simulation procedure, while the second approach uses the law of error propagation. The simulation procedure defines the impact of the imposed noise in the system measurements. Suppose that an initial surface and trajectory are given. Then a noise is added to the system measurements, and a surface is reconstructed through the LiDAR georeferencing equation. The differences between the initial and reconstructed coordinates of footprints determine the random error influence. The impact of a noise in the system measurements are mentioned below [65]:

- The position noise leads to similar noise in the derived point cloud. The effect is independent of the system flight altitude and scan angle.
- The orientation noise (platform attitude or encoder angles) affects the horizontal coordinates more than the vertical coordinates within the nominal scan angle ranges. The effect is dependent on the system flight altitude and scan angle.
- The noise in laser range mainly affects the vertical component of the derived coordinates (especially in the nadir region). The effect is independent of the system flight altitude but influences on the system's scan angle.

The second approach studies the stochastic characteristics of dependent variables based on the law of error propagation applied to the LiDAR georeferencing equation [66]. For the LiDAR footprint, the law of error propagation is used to estimate the precision of the derived coordinates based on the precision of the system measurements. Using this approach, one can choose the parameters, providing the best precision for the given system and flight configuration, especially for flat and horizontal solid surfaces. Such expected precision of the measurements can be estimated based on the LiDAR system manufacturing parameters. However, the manufacturing parameters do not consider vegetation and atmospheric effects.

The systematic biases in the system measurements (the encoder angles and laser ranges) and system parameters (the boresight angles and lever-arm offset relating the system components) lead to the systematic errors in the derived point cloud. Alike the random errors, the impact of systematic biases can be derived through mathematical analysis of the LiDAR georeferencing equation or using a simulation process. The impact of the various systematic biases of the LiDAR system on the ground may depend on the flight direction (forward and backward), the flight altitude, and the encoder angle (Table 2.2).

**Table 2.2** Impact of biases in the parameters and measurements of the LiDAR system with a linear scanner on the derived point cloud [65]

Type of bias	Flight altitude	Flight direction (forward/backward)	Encoder angle (across flight direction)
Biases in the lever-arm components	Effect is independent of the flight altitude	Planimetric effect is dependent on the flight direction Vertical effect is independent of the flight direction	Effect is independent of the encoder angle
Bias in the boresight pitch angle	Effect is dependent on the flight altitude	Planimetric effect along the flight direction is dependent on the flight direction	Effect is independent of the encoder angle
Bias in the boresight roll angle	Planimetric effect across the flight direction is dependent on the flight altitude Vertical effect is independent of the flight altitude	Planimetric effect across the flight direction and vertical effect are dependent on the flight direction	Planimetric effect across the flight direction is independent of the encoder angle Vertical effect is dependent on the encoder angle
Bias in the boresight yaw angle	Effect is independent of the flight altitude	Planimetric effect along the flight direction is independent of the flight direction	Planimetric effect along the flight direction is dependent on the encoder angle
Bias in the laser range measurements	Effect is independent of the flight altitude	Planimetric effect across the flight direction and vertical effect are independent of the flight direction	Planimetric effect ( $D_x$ ) across the flight direction and vertical effect ( $D_z$ ) are dependent on the encoder angle ( $D_x$ more than $D_z$ )
Bias in the encoder angle scale factor	Effect is dependent on the flight altitude	Planimetric effect across the flight direction and vertical effect are independent of the flight direction	Planimetric effect across the flight direction and vertical effect are dependent on the encoder angle

For a simulation process, a surface (usually flat) and a trajectory ought to be given. Then the biases are added to the system parameters and measurements in order to generate a bias-contaminated point cloud. The obtained point cloud is compared with the true surface in order to estimate the impact of the systematic errors. A compatibility of the overlapping strips is evaluated using two strips in forward and backward directions.

### 2.3.3 *Conventional LiDAR Calibration Methods*

The outcome of the LiDAR system is a point cloud, including 3D coordinates and, sometimes, the intensity values. The LiDAR georeferencing equation is a function of the boresight angles, lever-arm offset, and system measurements. Usually the calibration of the LiDAR system is required because of the biases of the system parameters. The Quality Assurance (QA) procedure helps to improve a quality of point cloud coordinates. The conventional calibration procedures require a full access to the raw measurements from the GPS/INS components and laser scanner as well as the use of control data. Notice that the vertical accuracy of LiDAR data is relatively high (5–30 cm) compared to other methodologies, while the horizontal accuracy is about 20–50 cm [67]. The quality of the LiDAR data is affected by many factors:

- Accuracy of the integrated GPS/INS position and orientation.
- Validity of the system parameters.
- Point density.
- Flight altitude and speed.
- Amount and density of vegetation and buildings.

The geometric and radiometric calibrations are differed. Referring to the guidelines in part 2 and part 3 of the VDI/VDE 2634 [68, 69], the accuracy of 3D optical measuring systems based on area scanning shall be evaluated by checking the equipment at regular intervals. This can be achieved by the length measurements and measurements in the same way of typical measurement objects. Sometimes, the measurements of sphere spacing error are reasonable. The precision of 3D laser scanning systems includes the errors in distance and angle measurements, and depends from the algorithm for fitting the spheres/targets in the point cloud. The influence of these errors is difficult to determine separately. The detailed information for the TLS systems one can find in [70].

Höfle and Pfeifer [3] introduced two different methods for correcting the laser scanning intensity data as the data-driven correction, when the predefined homogeneous areas are used to estimate empirically the best parameters for a given global correction function accounting all range-dependent influences, and the model-driven correction that improves the intensity values based on the physical principle of radar systems. For the data-driven correction, the parameters are

evaluated, using the Least-Squares Adjustment (LSA) method. For both approaches, a set of laser points with their corresponding plane positions ( $x, y, z$ ) and intensities  $I$  is required for reconstruction of a laser shot vector (direction and length) that is used for calculating the range and angle of an incidence.

For the data-driven correction, it is assumed that the recorded intensity is proportional to the ground reflectance and related to the flying height via empirical monotonic functions. It is considered that all physical effects are compensated, and the parameters calculated once can be used for further flights (with the same system settings and comparable atmospheric conditions). The general mathematical model has a view of Eq. 2.8, where  $I$  is an intensity,  $R$  is a range,  $I^{1000}$  is an intensity that is observed with  $R = 1000$  m,  $f(R)$  is an empirical function that can be represented by Eqs. 2.9 and 2.10 or other ones.

$$I(R) = I^{1000}f(R) \quad f(R) < f(R + \Delta R) \quad \forall \Delta R > 0 \quad f(1000) = 1 \quad (2.8)$$

$$f(R) = \frac{1}{k_1 R + (1 - 1000k_1)} \quad (2.9)$$

$$f(R) = \frac{1}{k_1 R + k_2 R^2 (1 - 1000k_1 - 1000^2 k_2)} \quad (2.10)$$

The parameters  $k_1$  and  $k_2$  are the unknown coefficients that are calculated from the series of experiments. Thus, if the functional relationship is quadratic, at least three notably different ranges are required. The measurements ought to be such that one echo is returned. This requirement is introduced in order to overcome an over-parameterization.

The model-driven correction is carried out under the following propositions:

- The reflectors are assumed to be the Lambertian reflectors.
- The surface slope can be estimated from a neighborhood of points.
- The atmospheric conditions are known and constant.
- The transmitted laser power is assumed to be constant.
- The incoming power is linear respect to the recorded intensity values.

The first two assumptions are fulfilled over an open terrain, while in the forests multiple reflections are the norm and it is impossible to obtain the measures close to physical properties. If all propositions are fulfilled, then the result is a value directly proportional to  $\rho$  and is impressed by Eq. 2.11, where  $\rho_{diffuse}(R_s, \alpha)$  is a value proportional to  $\rho$  normalized on standard range  $R_s$ ,  $I$  is a recorded intensity,  $R$  is a recorded range,  $\alpha$  is an angle of incident defined as angle between the surface normal and the incoming laser shot ray.

$$I(R_s) = \rho_{diffuse}(R_s, \alpha) \alpha \frac{R^2}{R_s^2} 10^{2Ra/10000} \frac{1}{\cos \alpha} \quad (2.11)$$

The coefficient  $a$  in Eq. 2.11 considers an average value for the atmosphere between airplane and ground. However, the atmospheric conditions during a flight may be complex. More sophisticated meteorological model ought to suppose that the coefficient  $a$  is a function of a range  $R$  and the absolute elevation  $z$  because the concentration of the scattering particles decreases with an altitude.

### 2.3.4 *Alternative LiDAR Calibration Methods*

The elimination of systematic errors provides a full potential accuracy of laser scanners. Bang [65] and Habib et al. [71] investigated the system parameters (including the mounting parameters) and the systematic errors in a laser scanner (the encoder angle scale factor and the laser range bias), using the point cloud coordinates of the overlapping strips. This leads to appearance of two alternative calibration methods that determined the biases in the system parameters and overcame the limitations of well-known calibration procedures of raw LiDAR data. The “simplified method” is applied in the case of the parallel overlapping strips, when the systematic biases are estimated using the identified discrepancies between the conjugate primitives in the overlapping LiDAR strips. The “quasi-rigorous method” deals with the non-parallel strips over a rugged terrain. This method requires the time-tagged LiDAR point cloud and the navigation data (trajectory position).

The simplified method is functioned under the following assumptions:

- Linear scanning systems are considered.
- Variations in the object space elevations are much smaller than the flight altitude.
- The flight lines are parallel.
- The platform trajectory is straight.
- Values of the roll and pitch angles are small enough to be ignored.
- Values of the boresight angles are assumed to be very small.

In contrast to the simplified method, the quasi-rigorous method deals with the non-parallel strips, heading variations and varying terrain elevations. It can be achieved by the use of the time-tagged point cloud and the trajectory position data. This method was developed under the following assumptions:

- Linear scanning systems are considered.
- Values of the roll and pitch angles are very small, and can be ignored.
- Values of the boresight angles are small, and can be ignored.

Unlike the simplified method, the quasi-rigorous method does not require the straight flight lines because the firing point position and heading are estimated by the trajectory position data and the time-tagged points.

The mathematical derivation for both methods may be found in the researches of Bang [65] and Habib et al. [71].

### 2.3.5 Equipment for Airborne Laser Scanning

The commercial civil companies, leaders in manufacturing of equipment for the ALS, are the Teledyne Optech, the Applanix POS AV, the TopoSys Harrier Model Range, the Riegl, the Leica, among others. Consider the products of the Teledyne Optech that has a wide family of laser scanners and digital cameras for the ALS systems.

Over the last 30 years, the Optech has proven that airborne surveying offers many advantages for acquiring spatially-located data across large areas [72]. From an aircraft's vantage point, the sensors capture the wide areas of terrain, such as cities, forests and farmlands, or long corridors such as power lines, railways, and rivers. Airborne sensors also have the speed and flexibility to survey many square kilometers in a single flight, even over rough or inaccessible terrain. The spheres of application are depicted in Fig. 2.2. The available Optech LiDAR systems are described in Table 2.3.

The Optech has a full line of airborne camera systems (from high resolution 80 megapixel RGB, to multispectral and thermal cameras) for a variety of applications in addition to being optimized for the LiDAR integration [73]. All airborne camera systems include a kinematic mounting for flexible configuration and a choice of interchangeable lenses to fit the specific flight requirements. The available Optech cameras are described in Table 2.4.

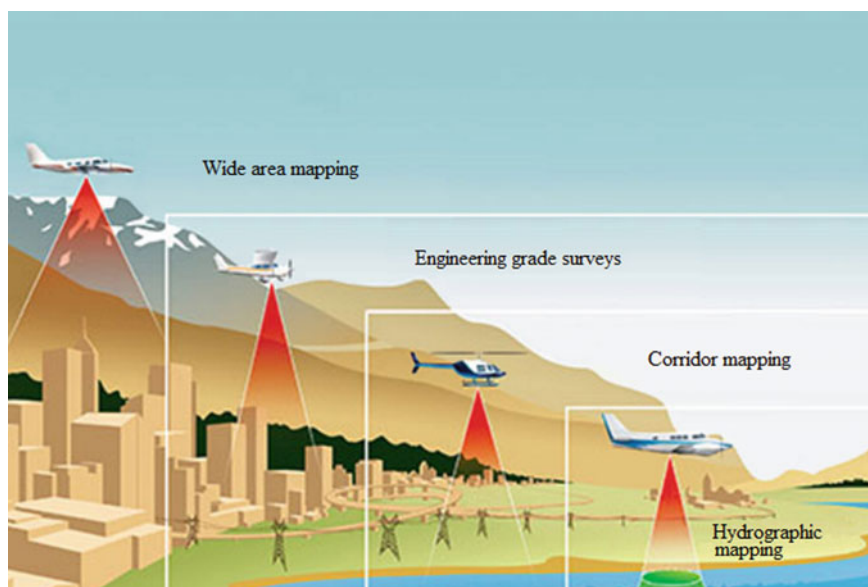




Fig. 2.2 Spheres of application in a schematic view (from [72])



Table 2.3 The Optech LiDAR systems from [72]

Title and assignment	Advantages	Applications	View
<p>The Optech Eclipse, autonomous LiDAR and imagery data collection</p> <p>Designed specifically for the efficient data collection of smaller project areas and corridor applications, the Optech Eclipse requires only a pilot for navigation. The Optech Eclipse combines an eye-safe, high-performance, 1.5-micron laser with a high-accuracy automatic imaging system. The LiDAR and image data are simultaneously captured on a single high-capacity removable Solid-State Drive (SSD) cartridge for fast and efficient data transfer to the Optech LiDAR Mapping Suite (LMS). The LMS includes both LiDAR and image pre-processing and employs robust least-squares algorithms to auto-calibrate LiDAR data</p>	<p>Fully autonomous airborne collection system for low-cost platforms</p> <p>Completely integrated active and passive imaging system</p> <p>Class 1 eye-safe laser for freedom of operation in environments</p> <p>Minimum of 4 points/m<sup>2</sup> from 1000 m (3300 ft) the above ground level (AGL)</p> <p>Up to 7 returns per shot for improved vertical density</p> <p>Rotating polygon scanner for parallel scan lines</p>	<p>Small-area surveying</p> <p>Power line mapping</p> <p>Pipeline monitoring</p> <p>Construction site monitoring</p> <p>Mine monitoring</p> <p>Stockpile surveying</p> <p>Archaeology and cultural heritage documentation</p>	 <p>The Optech Eclipse System</p>
<p>The Optech Galaxy</p> <p>The Optech Galaxy is the next generation of airborne solutions, packing more power and accuracy into a tiny footprint than any other sensor. Designed for everything from wide-area mapping to corridor surveys, the Optech Galaxy is truly a universal sensor that rivals larger systems with its ultra-dense data and industry-leading measurement precision and accuracy. The</p>	<p>550 kHz effective pulse repetition frequency (PRF)</p> <p>Up to 8 returns per pulse</p> <p>Fully programmable scanner provides a high point density at lesser field of view (FOV)</p> <p>Minimum target separation distance less than 0.7 m</p> <p>Wide dynamic range</p>	<p>Wide-area mapping</p> <p>Power line and transportation corridor</p> <p>Natural resource management</p> <p>Engineering and infrastructure modeling</p> <p>Urban mapping</p> <p>Defense and security</p>	 <p>The Optech Galaxy</p>

(continued)



Table 2.3 (continued)

Title and assignment	Advantages	Applications	View
Galaxy's new PulseTRAK and SwathTRAK technologies (patents pending) make surveying simpler than ever before by providing unique innovative feature sets that maximize productivity, increase information content and reduce overhead costs. The Optech Galaxy may be installed in a tactical UAV integrated in a helicopter pod for power line surveying or gyro-stabilized with an orthometric camera for a wide-area mapping	Real-time XYZI point clouds in LAS format Low power requirements and compact form factor Tight integration with the Teledyne Optech's modular line of digital cameras (RGB, NIR, thermal, and multispectral)		 The Optech Galaxy LiDAR sensor with optional GSM 4000
The Optech Titan The Optech Titan is a multispectral airborne LiDAR sensor that can be used day or night from complex environments. Whether it is high density topographic surveying, seamless shallow water bathymetry, environmental modeling, impervious urban surface mapping, or vegetative classification, the Optech Titan breaks new ground in active sensor design and performance. The Optech Titan's standard configuration includes three active beams with independent wavelengths of 532 nm, 1064 nm, and 1550 nm. Each beam has a 300 kHz effective sampling rate for a combined ground sampling rate of 900 kHz. A 29 MP fully-electronic interline camera provides high-resolution RGB imagery at frame rates >1 frame/s. The Optech CS-MS4100 has from 3 to 5 multispectral bands	900 kHz of high-density mapping capability Independent wavelengths, featuring "green" and NIR channels for topographic, shallow water bathymetry, vegetative mapping, and environmental modeling High-precision timing electronics, narrow laser pulse widths and beam divergences Fully programmable scanner 29 MP high-resolution, fully electronic QA camera Optional embedded 80 MP orthometric camera with a forward motion compensation Real-time XYZI point display	Topographic mapping Land cover classification Seamless shallow water bathymetry Environmental modeling Forest inventory and vegetative classification Natural resource management Disaster response	 The Optech Titan system

(continued)

Table 2.3 (continued)











Title and assignment	Advantages	Applications	View
<p>The Optech Orion</p> <p>The Optech Orion Airborne Laser Terrain Mapper is an ultra-compact total mapping solution with high data precision and accuracy. Modular components, direct upgrade options, and plug-and-fly passive imaging sensors deliver the scalable and flexible configurations. Three models of the Orion include:</p> <ul style="list-style-type: none"><li>- The Orion C is a low-altitude system for corridor and engineering mapping applications, such as power line, pipeline, and urban infrastructure surveying. The industry-leading ranging precision is of &lt;10 mm</li><li>- The Orion M is a low- to mid-altitude system provides a wider operational envelope enabling a wider range of applications including, urban modeling, engineering and transportation, and small topographic surveys</li><li>- The Orion H is a high-performance sensor used for the low-altitude corridor projects and/or high-altitude mountain surveys</li></ul>	<p>Compact form factor and low power requirements</p> <p>Exceptional small-target detection capability</p> <p>Real-time data monitoring with in-air LiDAR point cloud display and coverage maps</p> <p>Output XYZI point clouds in the LAS format in real-time</p> <p>Passive imaging capability with Optech's modular line of digital cameras (RGB, NIR, thermal, and multispectral)</p> <p>Flexible multi-sensor mounts for both helicopter and aircraft installations</p> <p>The consistent data quality and accuracy with production-focused workflow software with automated calibration capabilities</p>	<p>Corridor and asset</p> <p>Defense and security</p> <p>Natural resources</p> <p>Surveying and mapping (urban mapping)</p>	<div><p>The Optech Orion system</p><p>The Optech Orion with integrated camera in sled mount</p><p>The Optech Orion mounted in GSM</p></div>
<p>The Optech Pegasus</p> <p>The Optech Pegasus is a high-performance LiDAR mapping solution that is designed for maximum collection efficiency, data accuracy, and high point density.</p>	<p>Wide FOV coupled with the highest operating altitude and detect-ability</p> <p>High accuracy and precision deliver high-quality datasets</p>	<p>Natural resources</p> <p>Surveying and mapping (urban mapping, wide area mapping)</p>	<div></div> <p>(continued)</p>

Table 2.3 (continued)





Title and assignment		Advantages	Applications	View
<p>A multi-laser sensor, the Optech Pegasus includes a fully embedded, high-resolution orthometric camera and delivers extremely dense and information-rich datasets. The Optech Pegasus provides the highest point density and data accuracy at the lowest cost per square mile/km</p>	<p>The Optech Waveform Recorder</p> <p>The Optech Waveform Recorder provides waveform capture capability for all ALTM models. Benefits include true ground detection, increased return density, improved target separation distances, and improved classification results. This standalone configuration also enables the Optech Waveform Recorder to be moved from system to system as the need arises, giving surveyors the on-demand capability they need</p>	<p>Multi-laser design obtains twice the efficiency and data density of single-laser systems</p> <p>Fully-embedded, medium-format digital camera provides simultaneously-collected, high-resolution imagery</p>	<p>Natural resources (agriculture, environmental, forestry)</p>	<p>The Optech Pegasus system</p> 
		<p>High recording speeds provide data capture rates up to 300 kHz</p> <p>Intelligent digitizer automatically sub-samples collection rates above 100 kHz</p> <p>Detailed pulse amplitude and cross-section information</p> <p>Records only signals of interest (above user threshold) Real-time data display</p> <p>The SSD storage for unrestricted flight altitudes</p> <p>Timestamps waveforms with GPS time for synchronization with other altimeter data</p> <p>Accurate and precise datasets in the LAS 1.3 formats</p>		<p>The Optech Waveform Recorder</p> 

**Table 2.4** The Optech cameras (high-accuracy orthographic photography, thermal imaging, multispectral imaging) from [73]

Title and assignment	Advantages	Applications	View
<p>The Optech CS-10000 Aerial Digital Camera</p> <p>Standalone or integrated with LiDAR, the Optech CS-10000 is a complete corridor and small-area mapping solution. With 10,320 pixels across by 7760 pixels along the flight line, the Optech CS-10000 delivers a breathtaking imagery for detailed feature visualization and accurate engineering applications. Based on the patented technologies and advanced camera engineering, the Optech CS-10000 is optimized for both standalone imaging and the LiDAR integration</p>	<p>Field-replaceable shutter</p> <p>Interchangeable lenses</p> <p>Kinematic mounting for precise positioning</p> <p>The global system mobile (GSM) and sled mounts for configuration with the LiDAR sensors</p> <p>Batch processing provides the efficient imaging workflows</p> <p>80-Mpixel sensor with superior Ground Sample Distance (GSD) capacity</p>	<p>Corridor and asset (asset management, utilities)</p> <p>Defense and security</p> <p>Engineering (rail)</p> <p>Natural resources</p> <p>Surveying and mapping (digital photogrammetry, disaster management, urban mapping)</p>	 <p>The Optech CS-10000 camera</p>  <p>The Optech CS-10000 camera system</p>  <p>The Optech CS-10000 Camera with the Optech Orion LiDAR</p>
<p>The Optech CS-6500 Aerial Digital Camera</p> <p>The Optech CS-6500 is a stable, scalable, and versatile camera in a small and reliable form factor. Benefits include the LiDAR</p>	<p>Electronic shutter for extremely fast frame rates</p> <p>Interchangeable lenses to fit expanding business needs</p> <p>Metric quality data results deliver accuracy</p>	<p>Corridor and asset (asset management, pipelines, utilities)</p> <p>Defense and security (tactical surveillance and Intel)</p> <p>Engineering (rail)</p>	 <p>The Optech CS-6500 camera</p>




(continued)

Table 2.4 (continued)

Title and assignment	Advantages	Applications	View
integration, flexibility, market differentiation, and ability to expanded project needs. A field of view of 6500 pixels across by 4300 pixels along the flight line delivers more efficient survey flights. The Optech CS-6500 is seamlessly integrated with other Optech LiDARs and cameras to create a unique airborne imaging solution	Designed for integration with the LiDAR and other cameras	Surveying and mapping (urban mapping)	 The Optech CC-R camera controller
The Optech CS-LW640 Long-wave Thermal Camera The Optech CS-LW640 with other Optech cameras creates a unique airborne imaging solution. The Optech CS-LW640 is based on an uncooled micro-bolometer sensor with the resolution of $640 \times 480$ , and shares the core features of all Optech cameras. Integrated with the Optech Orion C LiDAR sensor platform, it is a proven and powerful tool for mapping thermal features in 3D thermal mapping	Long-wave infrared sensing expands possible mapping solutions Ruggedized construction for durability and custom mounting Kinematic mounting for precise alignment with the LiDAR and RGB cameras Geometric calibration and fast pre-processing	Corridor and asset (utilities) Defense and security Natural resources (environmental, forestry) Surveying and mapping (urban mapping)	 The Optech CS-LW640 thermal camera  The Optech CC-R camera controller
The Optech CS-MW640 Mid-wave Thermal Camera The Optech CS-MW640 with other Optech cameras creates a unique airborne imaging solution. The Optech CS-MW640 is based on a photovoltaic MCT with a resolution of $640 \times 480$ , and shares the core features of all Optech cameras. This mid-wave	Mid-wave infrared sensing expands possible mapping solutions Kinematic mounting for precise alignment with the LiDAR and RGB cameras Geometric calibration and fast pre-processing Ruggedized construction leverages extensible CS-Series architecture	Corridor and asset (utilities) Defense and security Natural resources (environmental, forestry) Surveying and mapping (urban mapping)	 The Optech CS-MW640 thermal camera



(continued)

Table 2.4 (continued)

Title and assignment	Advantages	Applications	View
infrared camera is ideal for integration with the Optech Orion C LiDAR sensor platform for 3D thermal mapping			 The Optech CC-R camera controller
The Optech CS-MS1920 Aerial Digital Camera The Optech CS-MS1920 multispectral camera with other Optech cameras creates a unique airborne imaging solution. The Optech CS-MS1920 is based on a patented high-definition 3-Charge-Coupled Device (CCD) camera design with color-separating optics that works together with large-format progressive-scan CCD sensors to maximize image resolution, dynamic range, and FOV. The Optech CS-MS1920 camera is the preferred choice for specialized applications requiring true multispectral capabilities, and delivers the ultimate in digital imaging quality. The one-inch HD sensor format provides the large pixel and sensing area needed for wide coverage and high dynamic range. Advanced features such as exposure control and white balance maximize the usability. Video preview capability provides a convenient progressive scan real-time display	3, 4, and 5 spectral band configurations Ruggedized design and kinematic mounts for precise mounting Geometric calibration for superior image quality Designed for integration with the LiDAR and cameras 3 high-definition CCD with high dynamic range and 400–1000 nm sensitivity Prism beam splitter architecture with patented compensating optics Georeferenced solutions with batch pre-processing Custom filters and polarization option	Corridor and asset Defense and security Natural resources Surveying and mapping (disaster management, wide area mapping)	 The Optech CS-MS1920 multispectral camera  The Optech CC-R camera controller

(continued)

Table 2.4 (continued)

Title and assignment	Advantages	Applications	View
<p>The Optech D-8900 Aerial Digital Camera</p> <p>With a footprint of 8900 pixels across by 6700 pixels along the flight line, the Optech D-8900 aerial digital camera is tightly integrated with the Optech Pegasus ALTM, and delivers accurate and precise imagery. A wide range of lens and filter options supports easy reconfiguration for specialized projects and applications</p>	<p>Extended acquisition windows</p> <p>True metric performance</p> <p>Adaptable and flexible with interchangeable lenses</p> <p>Robust controller for operational flexibility</p> <p>Improved workflow</p> <p>Improved time to delivery</p> <p>Simplified service and maintenance</p>	<p>Corridor and asset (asset management, utilities)</p> <p>Engineering (rail)</p> <p>Surveying and mapping (disaster management, urban mapping)</p>	<div><p>The Optech D-8900 camera</p><p>The Optech D-8900 camera controller and tablet</p></div>

Notice that a fusion of the LiDAR data and an imagery of any type is not a trivial task due to different nature of laser and video shooting [74, 75]. The detailed information about equipment for the ALS systems one can find in the corresponding sites, e.g., [76–79].

## 2.4 Overview of UAV Laser Scanning

Initially, the UAVs were introduced for the remote area investigation and mapping initially for military purpose. However, with the development of low-cost and light-weight sensors, the UAV systems became capable of carrying GPS, the Inertial Measurement Unit (IMU), and camera to serve a variety of civil applications, such as vegetation control [80], forest inventory [24], changing rivers [81], coastal flooding analysis [10], ice surface observation [82], forest fire monitoring [83], automatic detection of heat losses in buildings [84], etc. Nagai et al. [85] presented the UAV LiDAR system and direct georeferencing technique to process the LiDAR data for digital 3D modelling. Lin et al. [86] created a small helicopter system (4.5 kg) that is able to lift up a payload of 7 kg, including GPS/IMU, LiDAR, CCD camera, and thermal camera. This system had a wide scale mapping applications, such as the tree height estimation, the pole detection, the road extraction, and the DTM generation. Lin et al. [87] combined the data collected from the UAV imaging system and mobile mapping system for land cover classification in the urban environment. However, such issues as system calibration, sensor modelling, data fusion with onboard camera, and on-line data processing do not solved fully yet.

The particular qualities of UAV laser scanning are represented in Sect. 2.4.1, while the equipment for UAV laser scanning is performed in Sect. 2.4.2.

### 2.4.1 *Particular Qualities of UAV Laser Scanning*

The UAV is navigated by a small onboard GNSS/INS module. The main components of the own navigation module include the gyroscopes for measurement of angular velocity, the air pressure sensor, the magnetometer, and the accelerometer. The mission planning (flight path, flying height, velocity, and aims) is prepared using the ground station before a flight. The mission is executed fully automated but a wireless communication allows to track the actual position of the UAV and adapt the flight plan if it is possible. A pseudo-automatic or manual mode, e.g., for landing, is possible in the case of a signal loss or other unexpected problems. Flight-attitude data are logged and either transmitted in real time to the ground station or downloaded after the flight.

Because of limited payload and place, the restricted number of devices can be mounted on the UAV. Usually the UAV is equipped with light-weight cameras that



deliver the images in high quality and resolution after the mission. However, the camera's parameters can be unstable during a flight that causes a necessity in hardware or software stabilization. For vegetation analyses, the small and light-weight models of multispectral/hyperspectral sensors, the NIR, and/or Consumer InfraRed (CIR) sensors, laser scanners, spectrometers, and laser distance rangars and radar sounder are maintained [88].

The georeferencing can be done in several ways:

- Direct georeferencing (the direct measurement of camera position and orientation for each image) can be done with flight attitude data from the GNSS/IMU module [89].
- Georeferencing using the ground control. For dense forest, the extensive field work is necessary for accurate measurements of ground control.
- Combination of the direct georeferencing and ground control for accurate evaluation of the exterior orientation parameters.



The topics of the UAV autonomous control [90], the GPS-denied navigation [91], and the path planning [92] are discussed widely in areas including robotics, mechatronics, computer vision, and computer science. However, at present a lot of the existing algorithms in literature have not been realized onboard of the UAV in real time. This is a crucial problem, especially for indoor navigation. The developments in the Unmanned Aerial System (UAS)-based remote sensing, focusing on various types of the UASs, are actively discussed in literature [24, 93, 94].

### ***2.4.2 Equipment for UAV Laser Scanning***

One of the greatest advantages of the UAV laser scanning is its high flexibility and the relatively low operational costs. The miniaturization of the sensors and the increasing reliability of the navigation systems make the UAVs an indispensable instrument for many applications. Consider the UAV equipment manufactured by one of the leader companies in the world (Table 2.5).


Miniaturization has led to smaller payloads of sensors, computers, communication devices, and power supplies that have allowed smaller UAVs to perform the same functions as larger UAVs. Nowadays, nano-UAV (NUAV), micro-UAV (MAV), and mini-UAV (MUAV) are designed for military and civil purposes. Mini-UAVs are classified as man-portable, air-launched, and multi-mission devices [96]. Any UAV with a wingspan less than 2 m but greater than 30 cm is considered the MUAV. The MUAVs are suitable for military applications, such as for Intelligence, Surveillance, and Reconnaissance (ISR) missions, Nuclear, Biological, and Radiological (NBR) detection, communications relay, wiretapping, radar interference, and operations in cities and high-density population areas. The MAV is any UAV that has a wingspan of 30 cm or smaller. The MAVs are useful for battlefield reconnaissance, air monitoring, the NBR detection, target identification,

Table 2.5 The UAV equipment from [95]

Title and assignment	Advantages	Applications	View
<p>The RIEGL VUX-IUAV survey-grade unmanned laser scanner</p> <p>The RIEGL VUX-IUAV is a very lightweight and compact laser scanner, meeting the challenges of emerging survey solutions. Specifications include:</p> <ul style="list-style-type: none"><li>– 10 mm survey grade accuracy</li><li>– 5 mm precision</li><li>– Operating flight altitude up to more than 1000 ft</li><li>– Field of view up to 330°</li><li>– Scan speed up to 200 scans/s</li><li>– Eye safe operation at Laser Class 1</li><li>– Main dimensions: 227 mm × 180 mm × 125 mm</li><li>– Weight: 3.5 kg (without cooling fan device)/3.75 kg (with cooling fan device)</li></ul>	<p>Regular point pattern, perfectly parallel scan lines</p> <p>Cutting edge the Riegl technology, providing echo signal digitization, online waveform processing, and multiple-time-around processing</p> <p>Multiple target capability, practically unlimited number of targets echoes</p> <p>Electrical interfaces for the GPS data string and Sync Pulse</p> <p>LAN-TCP/IP interface</p> <p>Scan data storage on internal 240 GByte SSD memory</p>	<p>Agriculture and forestry</p> <p>Archaeology and cultural heritage documentation</p> <p>Corridor mapping: power line, railway track, and pipeline inspection</p> <p>Topography in open-cast mining</p> <p>Construction-site monitoring</p> <p>Surveying of urban environments</p> <p>Resource management</p>	 <p>The RIEGL VUX-IUAV survey-grade unmanned laser scanner</p>
<p>The RIEGL VQ-480-U lightweight airborne unmanned laser scanners</p> <p>The V-Line Airborne Laser Scanner RIEGL VQ-480-U provides high speed data acquisition, using a narrow infrared laser beam and a fast line scanning mechanism. A high-accuracy laser ranging is based on the Riegl's unique echo digitization and online waveform processing. The scanning mechanism is based on a fast rotating multi-facet polygonal mirror. Specifications include:</p>	<p>High-accuracy ranging based on echo digitization and online waveform processing</p> <p>High laser repetition rate, fast data acquisition</p> <p>Multiple target capability, unlimited number of targets</p> <p>Perfectly linear scan lines</p> <p>Compact, rugged, and very lightweight design</p> <p>Electrical interfaces for the GPS data string and Sync Pulse</p>	<p>Topography and mining</p> <p>Corridor mapping</p> <p>Power line inspection</p> <p>Archaeology and cultural heritage</p> <p>Target classification</p>	 <p>The RIEGL VQ-480-U lightweight airborne unmanned laser scanners</p>


(continued)

Table 2.5 (continued)

Title and assignment	Advantages	Applications	View
<ul style="list-style-type: none"><li>– 50–550 kHz laser pulse repetition rate</li><li>– 25 mm accuracy</li><li>– 25 mm precision</li><li>– 10 m minimum range</li><li>– Field of view 60°</li><li>– Eye safe operation at Laser Class 1</li><li>– Main dimensions: 347.5 mm × 183 mm</li><li>– Weight: 7.5 kg (without optional mounting frame; weight mounting frame: approx. 1 kg)</li></ul>	<p>Mechanical interface for the IMU mounting</p> <p>Integrated TCP/IP Ethernet interface</p>		
<p>The RIEGL RiCOPTER with VUX-SYS</p> <p>The RIEGL VUX-SYS is a complete miniaturized airborne laser scanning system solution of low weight and compact size for flexible use in the UAS/UAV/RPAS, helicopter, gyrocopter and ultra-light aircraft installations. The system consists of the RIEGL VUX-1UAV laser scanner, an IMU/GNSS system, a control unit and up to 4 optional cameras. The excellent measurement performance of the RIEGL VUX-1UAV in combination with a precise fiber optic gyroscope and the GPS/GLONASS receiver results in survey grade measurement accuracy</p>	<p>The RIEGL RiCOPTER remotely piloted aircraft system equipped with the RIEGL VUX-SYS complete miniaturized, lightweight ALS System</p> <p>The RIEGL VUX-1UAV lightweight airborne laser scanner fully integrated (providing 230° FOV, an effective measurement rate up to 350,000 measurements/sec, and 10 mm accuracy) Fibre-optic gyroscope and the GPS/GLONASS receiver integrated</p> <p>Remote control via low-bandwidth data link</p> <p>Operates up to 2 digital cameras</p>	<p>Precision agriculture</p> <p>Topography in open-cast mining</p> <p>Terrain and canyon mapping</p> <p>Archaeology and cultural heritage documentation</p> <p>Surveying of urban environments</p> <p>Construction-site monitoring</p> <p>Corridor mapping (power line, railway track, and pipeline inspection)</p>	 <p>The RIEGL RiCOPTER with VUX-SYS</p>

(continued)

Table 2.5 (continued)

Title and assignment	Advantages	Applications	View
<p>The RIEGL RiCOPTER remotely piloted aircraft system</p> <p>The robust and reliable airborne scanner carrying platform provides full mechanical and electrical integration of sensor system components into aircraft fuselage. The extremely lightweight carbon fiber main frame, foldable propeller carrier arms, and shock-absorbing undercarriage enable stable flight, safe landings and handy transportation. The flight characteristics of the X-8 array octocopter are smooth and stable in hovering positions as well as in demanding flight maneuvers under challenging conditions. For surveying missions, the RIEGL RiCOPTER is equipped with the RIEGL VUX-SYS for RiCOPTER, comprising the RIEGL VUX-1UAV LiDAR sensor, a IMU/GNSS unit, a control unit, and up to four high-resolution cameras with overall maximum payload of 16 kg (sensors and power supply)</p>	<p>High performance X-8 array foldable octocopter</p> <p>Payload weight 16 kg (sensors and power supply)</p> <p>Maximum Take-off Mass (MTOM) &lt; 25 kg</p> <p>Flight endurance with maximum load 30 min</p> <p>Operating flight altitude AGL of &gt;500 ft (operational limits for civil unmanned aircraft according to national regulations)</p> <p>Cushioned landing legs and shock-absorbing undercarriage for stable flights and save landings</p> <p>Foldable propeller carrier arms, integrated carrying handle, and special box for transportation</p>	<p>Precision agriculture</p> <p>Topography in open-cast mining</p> <p>Terrain and canyon mapping</p> <p>Archaeology and cultural heritage documentation</p> <p>Surveying of urban environments</p> <p>Construction-site monitoring</p> <p>Corridor mapping (power line, railway track, and pipeline inspection)</p>	 <p>The RIEGL RiCOPTER remotely piloted aircraft system</p>

and communications relay. The MAVs also can be used to reconnoiter building interiors.

A swarm has been defined as “modeled flight that is biologically inspired by the flights of flocking birds and swarming insects” [97]. The studies of grouping UAVs began until the early 1990s. The main idea was that a swarm of the UAVs can be performed like a network of assets and complete missions that have been reserved for larger UAVs or manned aircraft. It is evident that the use of multiple mini-UAVs or micro-UAVs rather than a single large one increases the efficiency greatly. Also, a swarm of inexpensive mini-UAVs and micro-UAVs possesses a redundancy advantage: if one member of the swarm is lost in action, the rest part of the swarm continues to carry out the mission.

## 2.5 Overview of Terrestrial Laser Scanning

The spheres of the TLS measurements are restricted by the non-large areas of surveillance. Due to the dense point clouds, the TLS is successfully applied in biomass estimations for forestry needs [98]. Fixed-position (mounted on a tripod) terrestrial laser scanners offer a high potential for 3D mapping of smaller areas with high detail. The TLS is the most suitable technique for detailed modelling of individual trees and canopies, providing the basic tree parameters, such as the number and position of trees, Diameter-at-Breast Height (DBH), and tree height. However, this technique, as well as the use of the hand-held scanners, cannot be applied for each tree in the forest. The appearance of the mobile laser scanning systems extended the scale possibilities of such investigations. Another interesting application of the TLS is a measurement of rill erosion in natural volumes, such as the banks of rivers, the slopes, mountains, etc. [99].

The particular qualities of the TLS are discussed in Sect. 2.5.1, while the equipment for this type of laser scanning is represented in Sect. 2.5.2. Similar to the mentioned above sections, the particular qualities of a mobile laser scanning are considered in Sects. 2.5.3 and 2.5.4 provides the equipment for a mobile laser scanning.

### 2.5.1 *Particular Qualities of Terrestrial Laser Scanning*

The TLS allows to scan surfaces from different angles, producing a rather comprehensive point cloud with sub-centimeter resolution, as compared to the resolutions of a few points per square meter that is typical for the Global Positioning System (GPS) based surveys. The high sampling rate of 4–40 kHz and the possibility to register several overlapping point clouds enable to promote the rapid survey across hundreds of meters. Resolution, range, and sampling rate of the TLS

permit the seamless integration of the collected data, creating the highly accurate DEMs.

The principle of TLS is the following: a highly collimated laser beam scans over a predefined solid angle in a regular scanning pattern and measures the time of flight of the laser signal. The scanning range of the mid-range terrestrial system allows to conduct the distance measurements in interval 2–800 m. Maas et al. [100] analyzed the main tree parameters, such as reliability and precision of the DBH, tree height, and trunk profile obtained by use of the TLS system. Five different study areas with varying scan parameters were used during the experiments. It was found that:

- An accuracy of tree detection was 97.5%.
- The DBH measurement accuracy determined with callipers ranged from 1.48 to 3.25 cm.
- The Root-Mean Square Error (RMSE) of the tree height measurements for different species was 4.55 m and remained 2.07 m, even with the removal of two outliers.

However, a quality of the TLS depends on the amount of object occlusion and the external environmental factors, such as wind or relative humidity (fog or light rain). The TLS in natural forest environments meets different levels of occlusion among the various vegetation components. The amount of occlusion depends on the width of the light beam, the point cloud density, and the use of the first or last return. Also, the resulting point clouds can be altered by the presence of a wind if the scanning time exceeds a few seconds. In the case of multiple scans from different viewpoints, a geometric scan registration adds another level of complexity to data pre-processing, reducing the adverse effects of object occlusion due to oversampling of areas. Côté et al. [101] proposed an architectural model of trees based on the following assumptions:


- The accounting of even small structural elements that can be resolved by the laser scanner (individual needles on a conifer).
- The lack of a priori information about leaf or shoot/needle inclination.
- The sophisticated distinguishing of wood and foliage from point cloud data.

In cases when the TLS data set is used, the 3D modelling of tree architecture is highly dependent on the scan acquisition parameters and data quality. Such constraints limit the efforts to model 3D tree architecture, especially for the coniferous species because they can be scanned already with the needles.

### ***2.5.2 Equipment for Terrestrial Laser Scanning***


Consider the equipment for the TLS manufactured by one of the leader companies in the world (Table 2.6).

Table 2.6 The terrestrial equipment from [102]

Title and assignment	Advantages	Applications	View
<p>The RIEGL VZ-400i 3D laser scanning system</p> <p>The RIEGL VZ-400i is 3D laser scanning system that combines an innovative new processing architecture, internet connectivity, and a suite of MEMS sensors with Riegl's latest laser scanning engine technology. The real-time data flow is enabled through dual processing platforms. The first platform includes a dedicated processing system for data acquisition, waveform processing, and system operations. The second processing platform enables the real-time data registration, georeferencing, filtering, and analysis to be executed simultaneously. The RIEGL VZ-400i harnesses this power by streaming it in real time via the integrated 3G/4G/LTE modem, WiFi, Bluetooth, and Ethernet communications hardware. With its integrated gyroscope, accelerometer, compass and barometer, the RIEGL VZ-400i's 1200 kHz pulse repetition rate can be fully utilized in nearly any environment and orientation. The system enables an incredible range of flexibility by providing support for numerous external peripherals and accessories via its integrated USB ports and stable mounting points</p>	<p>Processing architecture for data acquisition and simultaneous geo-referencing, filtering, and analysis in real time</p> <p>Cloud connectivity via Wi-Fi and 4G LTE</p> <p>High laser pulse repetition rate of up to 1.2 MHz</p> <p>Eye safe operation at Laser Class 1</p> <p>Wide field of view <math>100^{\circ} \times 360^{\circ}</math></p> <p>High speed data acquisition up to 500,000 measurements/s</p> <p>Range up to 800 m, accuracy 5 mm</p> <p>Multiple target capability for an unlimited number of target echoes</p> <p>Optional full waveform data output</p>	<p>Architecture and facade measurements</p> <p>As-built surveying</p> <p>Archaeology and cultural heritage</p> <p>City modeling</p> <p>Tunnel surveying</p> <p>– Civil engineering</p> <p>Forestry</p> <p>Monitoring</p> <p>Research</p> <p>Topography</p>	 <p>The RIEGL VZ-400i 3D laser scanning system</p>

(continued)


Table 2.6 (continued)

Title and assignment	Advantages	Applications	View
<p>The RIEGL VZ-400 3D laser scanner with online waveform processing</p> <p>This system provides high speed, non-contact data acquisition, using a narrow infrared laser beam and a fast scanning mechanism. High-accuracy laser ranging is based upon the Riegl's unique echo digitization and online waveform processing that allows achieving superior measurement capability even under adverse atmospheric conditions and the evaluation of multiple target echoes. The line scanning mechanism is based upon a fast rotating multi-facet polygonal mirror. The RIEGL VZ-400 is a very compact and lightweight surveying instrument</p>	<p>Up to 122,000 measurements/s</p> <p>5 mm accuracy and 3 mm repeatability</p> <p>600 m range</p> <p>1.5 m minimum range</p> <p>The Field of view 100° vertical/360° horizontal</p> <p>Eye safe operation at Laser Class 1</p> <p>Main dimensions:</p> <p>180 mm × 203 mm × 308 mm</p> <p>Integrated GPS receiver with antenna</p> <p>Various interfaces (LAN, WLAN, USB 2.0)</p> <p>Weight 9.6 kg</p>	<p>Street and railway mapping</p> <p>City modeling</p> <p>Mapping of coastal lines</p> <p>Power lines</p> <p>Civil engineering</p>	 <p>The RIEGL VZ-400 3D Laser scanner with online waveform processing</p>

(continued)




Table 2.6 (continued)

Title and assignment	Advantages	Applications	View
<p>The RIEGL VZ-1000 3D terrestrial laser scanners with online waveform processing</p> <p>This system provides high speed, non-contact data acquisition for ranges more than 1400 m, using a narrow infrared laser beam and a fast scanning mechanism. High-accuracy laser ranging is based upon the Riegl's unique echo digitization and online waveform processing that allows achieving superior measurement capability even under adverse atmospheric conditions and the evaluation of multiple target echoes. The line scanning mechanism is based upon a fast rotating multi-facet polygonal mirror. The RIEGL VZ-1000 is a very compact and lightweight surveying instrument</p>	<p>122,000 measurements/s, 300 kHz laser pulse repetition rate</p> <p>8 mm accuracy and 5 mm precision</p> <p>1400+ m range</p> <p>2.5 m minimum range</p> <p>The Field of view 100° vertical/360° horizontal</p> <p>Eye safe operation at Laser Class 1</p> <p>Main dimensions: 200 mm × 203 mm × 308 mm</p> <p>Integrated GPS receiver with antenna</p> <p>Various interfaces (LAN, WLAN, USB 2.0)</p> <p>Weight 9.8 kg</p>	<p>Topography and mining</p> <p>Archaeology and cultural heritage</p> <p>As-built surveying</p> <p>Monitoring</p>	 <p>The RIEGL VZ-1000 3D terrestrial laser scanners with online waveform processing</p>


(continued)

Table 2.6 (continued)

Title and assignment	Advantages	Applications	View
<p>The RIEGL VZ-2000 long-range high speed 3D laser scanners</p> <p>The V-Line 3D Laser Scanner RIEGL VZ-2000 is characterized by an extremely high measurement rate offering high accuracy data acquisition up to 400,000 measurements/s and up to 240 scan lines/s. The scanner further offers exceptional long range measurement performance of more than 2000 m to natural surfaces, while still maintaining completely eye safe operation (Laser Class 1). The Riegl's unique V-Line technology based on echo digitization, online waveform processing, and multiple-time-around processing is the key to enabling such high speed, long range, high accuracy measurements even in poor visibility and demanding multi-target situations caused by dust, haze, rain, snow, etc.</p>	<p>Very long range up to more than 2,000 m</p> <p>8 mm accuracy and 5 mm precision</p> <p>Very high effective measurement rate up to 400,000 measurements/s</p> <p>Eye safe operation in Laser Class 1</p> <p>Wide FOV 100° × 360°</p> <p>Main dimensions:</p> <p>196 mm × 203 mm × 308 mm</p> <p>Integrated L1 GPS receiver with antenna</p> <p>Various interfaces (LAN, WLAN, USB 2.0)</p> <p>Weight 9.9 kg</p>	<p>Surveying in open-pit mining</p> <p>Measurement of bulk materials</p> <p>Civil engineering</p> <p>City modeling</p> <p>Mapping of construction sites and construction-site monitoring</p> <p>Archaeology and cultural heritage</p> <p>Monitoring Topography and mining</p>	 <p>The RIEGL VZ-2000 long-range high speed 3d laser scanners</p>


(continued)

Table 2.6 (continued)

Title and assignment	Advantages	Applications	View
<p>The RIEGL VZ-4000 3D terrestrial laser scanners with online waveform processing</p> <p>This 3D RIEGL VZ-Line Laser Scanner offers superior and unrivaled long range measurement performance of up to 4000 m reflectorless while still maintaining completely eye safe operation (Laser Class 1). The Riegl's unique V-Line technology is based on echo digitization and online waveform processing and is the key to enabling such extreme long range measurements.</p> <p>The RIEGL VZ-4000 operates even in poor visibility and demanding multi-target situations caused by dust, haze, rain, snow, etc. that are frequently found in difficult environments such as mine sites</p>	<p>Very long range up to 4000 m</p> <p>15 mm accuracy and 10 mm precision</p> <p>4000 m range</p> <p>5 m minimum range</p> <p>Eye safe operation in Laser Class 1</p> <p>Wide FOV 60° × 360°</p> <p>High speed data acquisition up to 222,000 measurements/s</p> <p>Main dimensions: 248 mm × 226 mm × 450 mm</p> <p>Built-in calibrated digital camera</p> <p>Integrated L1 GPS receiver with antenna</p> <p>Built-in SSD data storage media</p> <p>Weight 14.5 kg</p>	<p>Topography and mining</p> <p>Monitoring</p> <p>Civil engineering</p> <p>Archaeology and cultural heritage</p>	 <p>The RIEGL VZ-4000 3D terrestrial laser scanners with online waveform processing</p>

(continued)

Table 2.6 (continued)

Title and assignment	Advantages	Applications	View
<p>The RIEGL VZ-6000 3D ultra long-range terrestrial laser scanners with online waveform processing</p> <p>The high speed, high resolution terrestrial 3D Laser Scanner RIEGL VZ-6000 offers an extremely long measurement range of more than 6000 m for topographic applications. Being the Laser Class 3B companion to the RIEGL VZ-4000, it is, due to its laser wavelength, exceptionally well suited for measuring snowy and icy terrain in glacier mapping and monitoring applications in mountainous regions. The RIEGL VZ-6000 is compatible with the well-proven Riegl software package RiSCAN PRO for terrestrial laser scanning, the Riegl's interface library RiVLiB, as well as the workflow-optimizing software packages RiMONITOR and RiMINING</p>	<p>Ultra long range up to 6000 m</p> <p>Up to 222,000 measurements/s</p> <p>15 mm accuracy and 10 mm precision</p> <p>6000 m range</p> <p>5 m minimum range</p> <p>The FOV 60° vertical/360° horizontal</p> <p>Main dimensions: 248 mm × 226 mm × 450 mm</p> <p>Integrated L1 GPS receiver with antenna</p> <p>Built-in calibrated digital camera</p> <p>Built-in SSD data storage media</p> <p>Weight approx. 14.5 kg</p>	<p>Glacier and snowfield mapping</p> <p>Topography and mining</p> <p>Monitoring</p> <p>Civil engineering</p> <p>Archaeology and cultural heritage</p>	 <p>The RIEGL VZ-6000 3D ultra long-range terrestrial laser scanners with online waveform processing</p>

A description of some other specifications for the TLS instruments, such as FARO LS 880HE80, Leica HDS6100, and Sick LMS151 as well as their application in experiments, one can find in [103].

### ***2.5.3 Particular Qualities of Mobile Laser Scanning***

The Mobile Laser Scanning (MLS) is a new technology at that the objects are continuously mapped by laser distance measurement from driving vehicles (such as a multi-van pickup, the Suburban Utility Vehicle (SUV), or even a ship or railway train), and transformed into 3D point cloud, using the GPS/IMU data. A comparison to the laser mapping technologies, like the ALS and the TLS, shows that the MLS combines components of both ALS and TLS. Angle of view, high point density and genuine 3D data are comparable with the TLS. Georeferencing capability and efficiency (in the sense of speedy mapping of large areas) are comparable characteristics of the ALS. Just like the ALS and the TLS, the MLS allows to combine the laser scanners with the RGB cameras in order to collect image data simultaneously with the laser data and to georeference them. A mobile mapping is expected to provide ease of mobilization and low costs in comparison to an airborne laser scanning. Especially, the MLS is attractive for projects, involving small areas and specific tasks. The current fields of the civil MLS application are the following:

- Inventory data collection for urban planning.
- Inventory-taking for the GIS applications (road inventory, road condition, tree register, lighting register, traffic sign register, railways inventory).
- Basic information for navigation (abnormal load transports).
- Basic information for modelling (volume control, facade documentation).

One of the most important operations for railways is the maintenance of infrastructures and mapping its surroundings for actual information. These operations need to be fast, accurate, and reliable for planning. The MLS technology is the most effective way of capturing the high resolution data. Due to the high volume of captured data, a post processing is very time consuming and labor intensive. In order to process the data effectively, the automatic solutions are required. The example of railways extraction is depicted in Fig. 2.3.

### ***2.5.4 Equipment for Mobile Laser Scanning***

Typical mobile LiDAR system consists of one or more laser scanners and digital cameras mounted on a vehicle (car, tram, or others). In the outdoor spaces, the trajectory of a vehicle is determined using the GPS and the high-grade IMU. Often

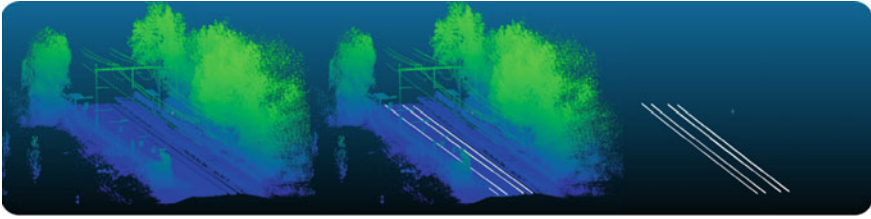


**Fig. 2.3** Extraction of railways from LiDAR data from [104]

a wheel rotation sensor is added to obtain the odometry data. However, this type of system cannot be directly used for indoor applications because the GPS is not available indoors.



The MLS systems have been commercially available for several years and can achieve an accuracy of a few tens of mm in range 400 m [105]. Consider the equipment for the MLS manufactured by one of the leader companies in the world (Table 2.7).

One can mention other mobile scanners, e.g., the Trimble MX8 [107]. This device is a premium mobile spatial imaging system capturing fully synchronized, high-quality georeferenced point clouds and high-resolution imagery. The vehicle-mounted system is designed for surveyors, engineers, and geospatial professionals conducting as-built modeling, inventory, inspection, encroachment analysis, and asset management for roadways, bridges, railway, utilities and other infrastructure management. The main features are the following:

- Performance 360° mobile dual laser scanners collecting over one million points per second.
- High-frequency digital cameras at set orientations, capturing the high resolution panorama and surface imagery.
- The POS LV positioning and orientation system, delivering extremely fast position updates (up to 200 Hz) and high accuracy results, even when the Global Navigation Satellite System (GNSS) signals are interrupted.
- Rigidly mounted and fully calibrated pod with a wide navigation and sensor base for easy installation on a variety of vehicle types.
- Trimble Trident software to extract survey, the GIS and construction deliverables.



The given above classification may be extended by additional types of laser scanning, such as the Hand-Held Mobile Laser Scanning (HMLS) or a use of the Ground-Penetrating Radar (GPR). The HMLS has the outstanding ability to collect the topographic data in complex terrains, combining the inherent scale and reliability of laser techniques with the flexibility of on-foot surveying and the typical for scanning systems density of point cloud. At present, the HMLS has a maximum laser range of 30 m and utilizes a structured light measurement approach with ranges of up to 1–5 m. The automated 3D scene reconstruction from the raw data is

**Table 2.7** The mobile equipment from [106]

Title and assignment	Advantages	Applications	View
<p>The RIEGL VMX-1HA high performance dual scanner mobile mapping system</p> <p>The RIEGL VMX-1HA is a high speed, high performance dual scanner mobile mapping system that provides dense, accurate, and feature-rich data at highway speeds. With 2 million measurements and 500 scan lines per second, this turnkey solution is ideally suited for survey-grade mobile mapping applications. This powerful technology comprises two RIEGL VUX-1HA High Accuracy LiDAR sensors and a high performance INS/GNSS unit. Optional camera systems complement the LiDAR data with precisely georeferenced images. Seamless Riegl workflow for the MLS data acquisition, processing, and adjustment is provided by the Riegl's proven software suite</p> <p>The RIEGL VMX-1HA RAIL</p> <p>With the RIEGL VMX-1HA-RAIL, the Riegl offers a proven, fully integrated high speed mobile laser scanning system for the demanding field of railway applications. It provides acquisition of a 360° field of view recording trackage, overhead wiring, rail heads and the complete periphery. The corresponding Riegl software packages offer comfortable features in data acquisition and processing and provide direct interfacing to third-party software packages to get main outcomes like clearance analysis, collision detection with train passage simulations, axis based measurements and surface monitoring, e.g., tunnel analysis</p>	<p>High laser pulse repetition rate of up to 2 MHz 500 scan lines per second Range 420 m Eye safe operation at Laser Class 1 The FOV 360° Multiple target capability Optional integration of up to 6 cameras Aerodynamically-shaped protective cover</p>	<p>Transportation infrastructure mapping Rail mapping Road surface measurements City modeling Rapid capture of construction sites and bulk material Surveying in open-pit mining GIS mapping and asset management As-built surveying</p>	<div></div> <p>The RIEGL VMX-1HA high performance dual scanner mobile mapping system</p>
	<p>Easy to mount lifting frame for fast installation by crane Additional mechanical interface for quick installation on various rail cars Main cable extensions for safe remote operation Optical distance measurement indicator optimized for railways Specially designed 19 inch rack based control module for fixed installation in a rail car Additional 230 V AC uninterruptible main power supply</p>	<p>Mapping of rail tracks and rail infrastructure Rapid safe data capture with minimal disruption to network schedules Clash detection Axis based measurements of rail infrastructure Clearance analysis</p>	<div></div> <p>The RIEGL VMX-1HA-RAIL</p>

(continued)



Table 2.7 (continued)

Title and assignment	Advantages	Applications	View
<p>The RIEGL VMQ-IHA high speed single scanner mobile mapping system</p> <p>The RIEGL VMQ-IHA is a compact, economically priced high speed single scanner mapping system, well suited for a variety of mobile mapping applications. The system consists of a measuring head, including one RIEGL VUX-IHA high accuracy LiDAR sensor, a compact control unit for system operation, and a special roof mount for convenient mounting. The optional integration of up to four cameras allows simultaneous acquisition of imagery to complement the captured LiDAR data. Seamless Riegl workflow for the MLS data acquisition, processing, and adjustment is provided by the Riegl's proven software suite</p>	<p>High laser pulse repetition rate of up to 1 MHz</p> <p>250 scan lines per second</p> <p>Range 420 m</p> <p>Eye safe operation at Laser Class 1</p> <p>The FOV 360°</p> <p>Multiple target capability</p> <p>Optional integration of up to 4 cameras</p>	<p>Transportation infrastructure mapping</p> <p>Road surface measurements</p> <p>City modeling</p> <p>Rapid capture of construction sites and bulk material</p> <p>As-built surveying and GIS mapping and asset management</p> <p>Surveying in open-pit mining</p>	 <p>The RIEGL VMQ-IHA high speed single scanner mobile mapping system</p>
<p>The RIEGL VUX-IHA compact rugged laser scanner</p> <p>The VUX-IHA high accuracy mobile scanning system is a very lightweight, compact and rugged laser scanner, that is easily mountable to whatsoever type of moving platform. It is perfectly suited for challenging survey missions based on cars, trains, robots, etc. This powerful technology comprises two RIEGL VUX-IHA high accuracy LiDAR sensors and a high performance INS/GNSS unit. The FOV of 360°, a very high laser pulse repetition rate of more than 1 MHz as well as an accuracy of 5 mm allow for excellent measurement results in applications like tunnel profile measuring, indoor and outdoor laser mapping, and railway applications</p>	<p>5 mm survey-grade accuracy</p> <p>Scan speed up to 250 scans/s</p> <p>Measurement rate up to 1,000,000 measurements/s</p> <p>The FOV of 360°</p> <p>Compact (227 × 180 × 125 mm), lightweight (3.5 kg), and rugged</p> <p>Electrical interfaces for the GPS data string and Sync Pulse</p> <p>LAN-TCP/IP interface</p> <p>Scan data storage on internal 240 GByte SSD memory</p>	<p>Indoor and outdoor laser mobile mapping</p> <p>Tunnel profile measurements</p> <p>Railway applications like clearance analysis</p>	 <p>The RIEGL VUX-IHA compact rugged laser scanner</p>

(continued)





Table 2.7 (continued)

Title and assignment	Advantages	Applications	View
<p>The RIEGL VMX-450 compact mobile laser scanners</p> <p>The RIEGL VMX-450 mobile laser scanning system offers extremely high measurement rates providing dense, accurate, and feature-rich data even at high driving speeds.</p> <p>The roof-carrier mounted measuring head integrates two RIEGL VQ-450 laser scanners as well as inertial measurement and GNSS equipment, housed under an aerodynamically-shaped protective cover. A camera platform ensures a setup of up to six digital cameras</p>		<p>Roadways mapping</p> <p>Rail corridors</p> <p>Waterways, ports, and harbors</p> <p>Monitoring of urban and vacant areas</p>	 <p>The RIEGL VMX-450 compact mobile laser scanners</p>
<p>The RIEGL VMX-450-RAIL railway mapping mobile laser scanners</p> <p>With the RIEGL VMX-450-RAIL, the Riegl offers a proven, fully integrated high speed mobile laser scanning system for the demanding field of railway applications. It provides acquisition of a 360° FOV recording trackage, overhead wiring, rail heads and the complete periphery. The fully-calibrated measuring head with optional camera system and open interfaces to various external sensors is combined with a lifting frame for crane installation and a mounting frame interface to different rail cars for quick and user-friendly system setup. The corresponding Riegl software packages offer comfortable features in data acquisition and processing and provide direct interfacing to third-party software packages for main applications</p>	<p>Easy to mount lifting frame for fast installation by crane</p> <p>Additional mechanical interface for quick installation on various rail cars</p> <p>Main cable extensions for safe remote operation</p> <p>Optical distance measurement indicator optimized for railways</p> <p>Specially designed 19 inch rack based control module for fixed installation in a rail car</p> <p>Additional 230 V AC uninterruptible main power supply</p>	<p>Mapping of rail tracks and rail infrastructure</p> <p>Rapid safe data capture with minimal disruption to network schedules</p> <p>Clash detection</p> <p>Axis based measurements of rail infrastructure</p> <p>Clearance analysis</p>	 <p>The RIEGL VMX-450-RAIL railway mapping mobile laser scanners</p>

(continued)

Table 2.7 (continued)

Title and assignment	Advantages	Applications	View
<p>The RIEGL VQ-450 mobile laser scanners with online waveform processing</p> <p>The V-Line “Full Circle” laser scanner RIEGL VQ-450 is a very high speed, non-contact profile measuring system using a narrow infrared laser beam and a fast line scanning mechanism, enabling full 360 degree beam deflection without any gaps. It is characterized by a Laser Pulse Repetition Rate (PRR) of up to 550 kHz and a scanning rate of up to 200 lines per second. Multi-target capability based on echo digitization and online waveform analysis offers superior measurement capabilities even under adverse atmospheric conditions</p>	<p>Very high laser PRR up to 550 kHz</p> <p>Very high scanning rate up to 200 lines/s</p> <p>Very long range up to 800 m</p> <p>High-accuracy ranging</p> <p>Multiple target capability, unlimited number of targets</p> <p>Perfectly linear scan lines</p> <p>Compact, rugged, and lightweight design</p> <p>Integrated LAN-TCP/IP interface</p>	<p>Street and railway mapping</p> <p>City modeling</p> <p>Mapping of coastal lines</p> <p>– Power lines</p> <p>Civil engineering</p>	 <p>The RIEGL VQ-450 mobile laser scanners with online waveform processing</p>
<p>The RIEGL VMZ hybrid 3D mapping mobile laser scanners</p> <p>The fully integrated, accurate, and compact the RIEGL VMZ hybrid mobile laser mapping system enables combined static and kinematic data acquisition, using a single RIEGL VZ-400, VZ-1000 or VZ-2000 laser scanner. This leads to lower mobilization costs and a high return on investment. Flexible setup, easy mounting, and a user-friendly workflow mobilize the Riegl 3D terrestrial laser scanner for applications like mapping of transportation infrastructure, city modeling, mine surveying, bulk measurements, etc.</p>	<p>The IMU/GNSS unit, fully integrated to support the RIEGL VZ-400(i), VZ-1000 and VZ-2000 scanners for mobile data acquisition</p> <p>Quick switch from mobile to terrestrial applications, and vice versa</p> <p>Image data acquisition with a calibrated and the GPS synchronized NIKON DSLR camera</p> <p>Additionally panoramic camera systems such as POINT GREY Ladybug are available</p> <p>Single power supply for VZ scanner and the IMU GNSS unit from a standard car battery</p> <p>Easy system operation with single laptop running RiACQUIRE</p>	<p>City modeling</p> <p>Surveying in open-pit mining</p> <p>Measurement of bulk materials</p> <p>Road surface scans</p> <p>Shore surveying and marine applications</p> <p>Civil engineering</p> <p>Topography</p> <p>Monitoring</p> <p>Facade modeling</p> <p>As-built surveying</p> <p>Architecture</p> <p>Archaeology</p>	 <p>The RIEGL VMZ hybrid 3D mapping mobile laser scanners</p>

carried out using the sophisticated Simultaneous Localization And Mapping (SLAM) algorithm that simultaneously computes the full trajectory of scanning and point cloud of surface measurements. The HMLS system works better in the indoor scenes with the static surfaces in comparison to the outdoor environments with highly irregular and covered with vegetation surfaces that cause more challenges during reconstruction [108]. Ryding et al. [109] demonstrated the efficiency of the HMLS system application in comparison to the conventional tripod TLS system. They show that the HMLS approach provides better survey coverage time per surveyor because the end-user can easily direct the scanner toward the points of interest and capture only the required data from the whole survey area.

The GPR is an established noninvasive (i.e., nondestructive) inspection method that has been used worldwide for more than thirty years to locate subsurface objects such as pipes, utilities, and other engineering and environmental targets. Bassuk et al. [110] proposed the methodology for locating of tree roots, using the GPR. The GPR employs the electromagnetic waves that reflect, refract and/or diffract from the boundary in a predictable manner in the boundaries between objects with different electro-magnetic properties of materials [111]. The benefits of a mapping tree roots based on the GPR measurements are the following:

- The method is capable of scanning root systems of large trees under field conditions in a relatively short time.
- The method is completely noninvasive and does not disturb the soils or damage the trees examined.
- The method allows the repeated measurements that reveal a long-term root system development.
- The method allows observation of root distribution beneath hard surfaces (e.g., concrete, asphalt, bricks, pavers, roads, buildings).
- The accuracy is sufficient to detect the structural roots with diameters till 1 cm.

Differences between the radar output and associated root counts in sample zones were found to be normally distributed in the CU-Structural Soil (CU-Structural Soil is a mixture of crushed gravel and soil with a small amount of hydrogel to prevent the soil and stone from separating during the mixing and installation process).

## 2.6 Comparison of Remote Sensing Techniques for Forest Inventory

The remote sensing data are successfully applied within the forestry industry, particularly, in computation of forest inventory metrics. The airborne and space-borne sensors provide the spatially explicit data collected from large areas. It is well-known that the spatial extent and resolution are inversely related that makes the precision and accuracy are suboptimal for many tasks [25, 112].

The ALS data of 3D canopy structure are captured at heights between 500 and 5000 m. The forest properties, such as biomass and the Leaf Area Index (LAI) at the stand level, are evaluated using these ALS data as the input data for corresponding methods [113, 114]. The detection of individual trees from the ALS data is difficult with the reported detection rates varying significantly (between 40 and 96%) [115–117]. The 3D segmentation techniques may improve the accuracy of the information derived from a tree-level analysis [115, 118]. However, the required accuracy of tree segmentation is still not sufficient to estimate a number of forest metrics. More, the bias toward large dominant trees can cause significant overestimation of final inventory values such as timber yield [119]. This means the necessity of acquisition of numerous statistical data from large forest areas with the following processing and evaluation with real inventory data [25].

The terrestrial remote sensing techniques have been deployed actively in forest inventory [100]. During the TLS, the woody components of the canopy are often visible that allows to estimate the key tree-level inventory metrics, such as the DBH, shape of trunk, and crown length, objectively and with high precision. However, the terrestrial techniques can be used to measure small forest areas only and also the data collected by the TLS instruments are highly affected by occlusions. Therefore, the multiple viewing points are required in order to avoid a downward bias in trunk detection. The MLS systems overcome the small area restriction of the TLS by deploying the laser scanner onboard a moving vehicle or using the hand-held scanner. These systems are promising in deriving of individual tree-level parameters [120] but require further investigation.

Recently, the UAV laser scanning has been proposed as a tool for mapping and measuring tree metrics [24]. These systems provide a low-cost data collection with point densities up to 1000 points per square meter. Jaakkola et al. [121] provided a pilot study, showing that the underestimation of tree height presents in both the ALS and the TLS, while it is significantly reduced within the UAV data. This effect may be explained by the increased point density of the point clouds in comparison to the ALS and the TLS. (Objectively, the scanner and the sensors mounted on the on-board UAV platforms have higher errors and different sources of error.) Wallace et al. [122, 123] verified the precision of forest metrics from the UAV data scanning in a eucalypt plantation forest. The results of the percent canopy cover analysis proved that the UAV scanning data can provide the fast, low-cost, and objective information in this scope.

## 2.7 Conclusions

Three main types of laser technique, such as the airborne, the UAV, and terrestrial laser scanning, were considered, beginning from the physical basics and ending the commercial laser scanning systems for civil applications. Each type of laser scanning has the own applications in dependence on the mission, the scale of a studying area, and financial possibilities of the end-users. At present, one can choose the

laser scanner that has a high suitability for decision of the given practical task. Also, it was shown that a forest inventory is one the most popular topic among other applications that apply the laser scanning technologies.

## References

1. Ackermann F (1999) Airborne laser scanning—present status and future expectations. *ISPRS J Photogramm Remote Sens* 54(2–3):64–67
2. Yan WY, Shaker A, El-Ashmawy N (2015) Urban land cover classification using airborne LiDAR data: a review. *Remote Sens Environ* 158:295–310
3. Höfle B, Pfeifer N (2007) Correction of laser scanning intensity data: data and model-driven approaches. *ISPRS J Photogramm Remote Sens* 62(6):415–433
4. LiDAR News. <http://blog.lidarnews.com/global-airborne-lidar-market-report/>. Accessed 31 July 2016
5. Webster TL, Forbes DL, Dickie S, Shreenan R (2004) Using topographic LiDAR to map flood risk from storm-surge events for Charlottetown, Prince Edward Island, Canada. *Can J Remote Sens* 30(1):64–76
6. Casas A, Benito G, Thorndycraft V, Rico M (2006) The topographic data source of digital terrain models as a key element in the accuracy of hydraulic flood modelling. *Earth Surf Proc Land* 31(4):444–456
7. Mallet C, Bretar F (2009) Full-waveform topographic LiDAR: state-of-the-art. *ISPRS J Photogramm Remote Sens* 64(1):1–16
8. Hancock S, Lewis P, Foster M, Disney M, Muller JP (2012) Measuring forests with dual wavelength LiDAR: a simulation study over topography. *Agric For Meteorol* 161:123–133
9. Renslow MS (2012) Manual of airborne topographic LiDAR. American Society for Photogrammetry and Remote Sensing
10. Webster TL, Forbes DL, MacKinnon E, Roberts D (2006) Flood-risk mapping for storm-surge events and sea-level rise using LidAR for southeast New Brunswick. *Can J Remote Sens* 32(2):194–211
11. Mason DC, Horritt MS, Hunter NM, Bates PD (2007) Use of fused airborne scanning laser altimetry and digital map data for urban flood modelling. *Hydrol Process* 21(11):1436–1447
12. Tsubaki R, Fujita I (2010) Unstructured grid generation using LiDAR data for urban flood inundation modelling. *Hydrol Process* 24(11):1404–1420
13. Arrighi C, Brugioni M, Castelli F, Franceschini S, Mazzanti B (2013) Urban microscale flood risk estimation with parsimonious hydraulic modelling and census data. *Nat Hazards Earth Syst Sci* 13:1375–1391
14. Garroway K, Hopkinson C, Jamieson R (2011) Surface moisture and vegetation influences on LiDAR intensity data in an agricultural watershed. *Can J Remote Sens* 37(3):275–284
15. Lim K, Treitz P, Wulder M, St-Onge B, Flood M (2003) LiDAR remote sensing of forest structure. *Prog Phys Geogr* 27(1):88–106
16. Chasmer L, Hopkinson C, Smith B, Treitz P (2006) Examining the influence of changing laser pulse repetition frequencies on conifer forest canopy returns. *Photogramm Eng Remote Sens* 72(12):1359–1367
17. Cuesta J, Chazette P, Allouis T, Flamant PH, Durrieu S, Sanak J, Genau P, Guyon D, Loustau D, Flamant C (2010) Observing the forest canopy with a new ultra-violet compact airborne LiDAR. *Sensors* 10(8):7386–7403
18. Hyypä J, Hyypä H, Leckie D, Gougeon F, Yu X, Maltamo M (2008) Review of methods of small-footprint airborne laser scanning for extracting forest inventory data in boreal forests. *Int J Remote Sens* 29(5):1339–1366

19. Lang MW, McCarty GW (2009) LiDAR intensity for improved detection of inundation below the forest canopy. *Wetlands* 29(4):1166–1178
20. Morsdorf F, Nichol C, Malthus T, Woodhouse IH (2009) Assessing forest structural and physiological information content of multi-spectral LiDAR waveforms by radiative transfer modelling. *Remote Sens Environ* 113(10):2152–2163
21. Korpela I, Orka HO, Hyypä J, Heikkinen V, Tokola T (2010) Range and AGC normalization in airborne discrete-return LiDAR intensity data for forest canopies. *ISPRS J Photogramm Remote Sens* 65(4):369–379
22. Allouis T, Durrieu S, Chazette P, Bailly JS, Cuesta J, Véga C, Flamant P, Couteron P (2011) Potential of an ultraviolet, medium-footprint LiDR prototype for retrieving forest structure. *ISPRS J Photogram Remote Sens* 66(6):S92–S102
23. Gatzliolis D (2011) Dynamic range-based intensity normalization for airborne, discrete return LiDAR data of forest canopies. *Photogramm Eng Remote Sens* 77(3):251–259
24. Wallace L, Lucieer A, Watson C, Turner D (2012) Development of a UAV–LiDAR system with application to forest inventory. *Remote Sens* 4(6):1519–1543
25. Wulder MA, White JC, Nelson RF, Næsset E, Ørka HO, Coops NC, Hilker T, Bater CW, Gobakken T (2012) LiDAR sampling for large-area forest characterization: a review. *Remote Sens Environ* 121:196–209
26. Bradbury RB, Hill RA, Mason DC, Hinsley SA, Wilson JD, Balzter H, Anderson GQ, Whittingham MJ, Davenport IJ, Bellamy PE (2005) Modelling relationships between birds and vegetation structure using airborne LiDAR data: a review with case studies from agricultural and woodland environments. *IBIS* 147(3):443–452
27. Hartfield KA, Landau KI, Van Leeuwen WJ (2011) Fusion of high resolution aerial multispectral and LiDAR data: land cover in the context of urban mosquito habitat. *Remote Sens* 3(11):2364–2383
28. Desikan P, Karunakaran K, Gokulnath G (2013) Design of an aquatic park and salvation of endangered aquatic species in its natural habitat. *APCBEE Procedia* 5:197–202
29. Jaboyedoff M, Oppikofer T, Abellan A, Derron MH, Loya A, Metzger R, Pedrazzini A (2012) Use of LIDAR in landslide investigations: a review. *Nat Hazards* 61(1):5–28
30. Haala N, Kada M (2010) An update on automatic 3D building reconstruction. *ISPRS J Photogramm Remote Sens* 65(6):570–580
31. Wang R (2013) 3D building modeling using images and LiDAR: A review. *Int J Image Data Fusion* 4(4):273–292
32. Rottensteiner F, Sohn G, Gerke M, Wegner JD, Breitkopf U, Jung J (2014) Results of the ISPRS benchmark on urban object detection and 3D building reconstruction. *ISPRS J Photogramm Remote Sens* 93:256–271
33. Quackenbush LJ, Im J, Zuo Y (2013) Road extraction: a review of LiDAR-focused studies. In: Wang G, Weng Q (eds) *Remote sensing of natural resources*. CRC Press, Boca Raton
34. Deems JS, Painter TH, Finnegan DC (2013) LiDAR measurement of snow depth: a review. *J Glaciol* 59(215):467–479
35. ASPRS LIDAR data exchange format standard, version 1.0. [http://www.asprs.org/wp-content/uploads/2010/12/asprs\\_las\\_format\\_v10.pdf](http://www.asprs.org/wp-content/uploads/2010/12/asprs_las_format_v10.pdf). Accessed 31 July 2016
36. LAS specification, version 1.1. [http://www.asprs.org/wp-content/uploads/2010/12/asprs\\_las\\_format\\_v11.pdf](http://www.asprs.org/wp-content/uploads/2010/12/asprs_las_format_v11.pdf). Accessed 31 July 2016
37. LAS specification, version 1.2. [http://www.asprs.org/wp-content/uploads/2010/12/asprs\\_las\\_format\\_v12.pdf](http://www.asprs.org/wp-content/uploads/2010/12/asprs_las_format_v12.pdf). Accessed 31 July 2016
38. LAS specification, version 1.3–R11. [http://www.asprs.org/wp-content/uploads/2010/12/LAS\\_1\\_3\\_r11.pdf](http://www.asprs.org/wp-content/uploads/2010/12/LAS_1_3_r11.pdf). Accessed 31 July 2016
39. LAS specification, version 1.4–R13. [http://www.asprs.org/wp-content/uploads/2010/12/LAS\\_1\\_4\\_r13.pdf](http://www.asprs.org/wp-content/uploads/2010/12/LAS_1_4_r13.pdf). Accessed 31 July 2016
40. Kaasalainen S, Hyypä J, Litkey P, Hyypä H, Ahokas E, Kukko A, Kaartinen H (2007) Radiometric calibration of ALS intensity. *Int Arch Photogramm Remote Sens Spat Inf Sci XXXVI, Part 3/W52*:201–205

41. Wagner W (2010) Radiometric calibration of small-footprint full-waveform airborne laser scanner measurements: basic physical concepts. *ISPRS J Photogramm Remote Sens* 65 (6):505–513
42. Charaniya A, Manduchi R, Lodha S (2004) Supervised parametric classification of aerial LiDAR data. In: IEEE 2004 conference on computer vision and pattern recognition workshop CVPRW 2004, vol 3, pp 1–8
43. Brennan R, Webster T (2006) Object-oriented land cover classification of LiDAR derived surfaces. *Can J Remote Sens* 32(2):162–172
44. Lodha SK, Kreps EJ, Helmbold DP, Fitzpatrick D (2006) Aerial LiDAR data classification using support vector machines (SVM). 3rd Int Symposium on 3D Data Processing, Visualization, and Transmission, pp 567–574
45. Farid A, Rautenkranz D, Goodrich DC, Marsh SE, Sorooshian S (2006) Riparian vegetation classification from airborne laser scanning data with an emphasis on cottonwood trees. *Can J Remote Sens* 32(1):15–18
46. Lodha S, Fitzpatrick D, Helmbold D (2007) Aerial LiDAR data classification using AdaBoost. In: 6th international conference on 3-D digital imaging and modeling 3DIM 2007, pp 435–442
47. Orka HO, Næsset E, Bollandsas OM (2007) Utilizing airborne laser intensity for tree species classification. In: *ISPRS workshop on laser scanning 2007 and SilviLaser 2007*, vol XXXVI, Part 3/W52, pp 300–304
48. Im J, Jensen JR, Hodgson ME (2008) Object-based land cover classification using high-posting-density LiDAR data. *GIScience Remote Sens* 45(2):209–228
49. Goncalves G, Seco L, Reyes F, Miranda D (2008) Land cover classification of rural areas using LiDAR data: a comparative study in the context of fire risk. In: 8th international conference on LiDAR applications in forest assessment and inventory *SilviLaser 2008*, pp 427–436
50. Kim S, McGaughey RJ, Andersen HE, Schreuder G (2009) Tree species differentiation using intensity data derived from leaf-on and leaf-off airborne laser scanner data. *Remote Sens Environ* 113(8):1575–1586
51. Habib A, Kersting A, Shaker A, Yan WY (2011) Geometric calibration and radiometric correction of LiDAR data and their impact on the quality of derived products. *Sensors* 11 (9):9069–9097
52. Yan WY, Shaker A, Habib A, Kersting AP (2012) Improving classification accuracy of airborne LiDAR intensity data by geometric calibration and radiometric correction. *ISPRS J Photogramm and Remote Sens* 67:35–44
53. Buján S, González-Ferreiro E, Reyes-Bueno F, Barreiro-Fernández L, Crecente R, Miranda D (2012) Land use classification from LiDAR data and ortho-images in a rural area. *Photogram Rec* 27:401–422
54. Shaker A, El-Ashmawy N (2012) Land cover information extraction using LiDAR data. *Int Arch Photogramm Remote Sens Spat Inf Sci* XXXIX-B7:167–172
55. Markets and Markets. <http://www.marketsandmarkets.com/Market-Reports/lidar-market-1261.html>. Accessed 31 July 2016
56. Hitz B, Ewin JJ, Hecht J (1998) Introduction to laser technology, 3rd edn. IEEE Press, New York
57. Weber MJ (1999) Handbook of laser wavelength. CRC Press, Boca Raton
58. Silfvast WT (2004) Laser fundamentals, 2nd edn. Cambridge University Press, Cambridge
59. Jelalian AV (1992) Laser radar systems. ArtechHouse, Boston
60. Rees WG (2001) Physical principles of remote sensing, 2nd edn. Cambridge University Press, Cambridge
61. Jutzi B, Stilla U (2006) Range determination with waveform recording laser systems using a Wiener Filter. *ISPRS J Photogramm Remote Sens* 61(2):95–107
62. Kim II, McArthur B, Korevaar E (2001) Comparison of laser beam propagation at 785 nm and 1550 nm in fog and haze for optical wireless communications. *Proc SPIE* 4214, Optical Wireless Communications III, 26. doi:[10.1117/12.417512](https://doi.org/10.1117/12.417512)



63. Lemmens M (2009) Airborne LiDAR sensors. *GIM Int* 23(2):16–19
64. Shan J, Toth CK (2009) Topographic laser ranging and scanning. CRC Press, Boca Raton
65. Bang KI (2010) Alternative methodologies for LiDAR system calibration. PhD dissertation, Calgary, Alberta
66. Mikhail EM, Ackerman F (1976) Observations and least squares. University Press of America, Lanham
67. McGlone JC, Mikhail EM, Bethel J, Mullen R (2004) Manual of photogrammetry, 5th edn. American Society for Photogrammetry and Remote Sensing, Bethesda
68. VDI. The Association of German Engineers. [http://www.vdi.eu/guidelines/vdivde\\_2634\\_blatt\\_2-optische\\_3\\_d-messsysteme\\_bildgebende\\_systeme\\_mit\\_flaechenhafter\\_antastung/](http://www.vdi.eu/guidelines/vdivde_2634_blatt_2-optische_3_d-messsysteme_bildgebende_systeme_mit_flaechenhafter_antastung/). Accessed 7 Aug 2016
69. VDI. The Association of German Engineers. [http://www.vdi.eu/guidelines/vdivde\\_2634\\_blatt\\_3-optische\\_3\\_d-messsysteme\\_bildgebende\\_systeme\\_mit\\_flaechenhafter\\_antastung/](http://www.vdi.eu/guidelines/vdivde_2634_blatt_3-optische_3_d-messsysteme_bildgebende_systeme_mit_flaechenhafter_antastung/). Accessed 7 Aug 2016
70. Cuartero A, Armesto J, Rodríguez PG, Arias P (2010) Error analysis of terrestrial laser scanning data by means of spherical statistics and 3D graphs. *Sensors* 10(11):10128–10145
71. Habib A, Bang KI, Kersting AP, Chow J (2010) Alternative Methodologies for LiDAR System Calibration. *Remote Sens* 2(3):874–907
72. Teledyne Optech. Airborne Survey. <http://www.teledyneoptech.com/index.php/products/airborne-survey/>. Accessed 3 Aug 2016
73. Teledyne Optech. <http://www.teledyneoptech.com/index.php/products/airborne-survey/camera-systems/>. Accessed 3 Aug 2016
74. Wang H, Glennie C (2015) Fusion of waveform LiDAR data and hyperspectral imagery for land cover classification. *ISPRS J Photogram Remote Sens* 108:1–11
75. Favorskaya M, Tkacheva A, Danilin IM, Medvedev EM (2015) Fusion of airborne LiDAR and digital photography data for tree crowns segmentation and measurement. In: Damiani E, Howlett RJ, Jain LC, Gallo L, De Pietro G (eds) Intelligent interactive multimedia systems and services. Springer International Publishing, Switzerland
76. Applanix. POS AV. <http://www.applanix.com/products/airborne/posav.html>. Accessed 3 Aug 2016
77. TopoSys Harrier Model Range. <http://www.gim-international.com/content/news/toposys-harrier-model-range>. Accessed 3 Aug 2016
78. RIEGL USA. <http://products.rieglusa.com/item/airborne-scanners/lms-q680i-long-range-laser-scanner/item-1001/>. Accessed 3 Aug 2016
79. Leica. LiDAR Sensors. <http://leica-geosystems.com/products/airborne-systems/lidar-sensors>. Accessed 3 Aug 2016
80. Ax M, Thamke S, Kuhnert L, Kuhnert KD (2013) UAV based laser measurement for vegetation control at high-voltage transmission lines. *Adv Mater Res* 614–615:1147–1152
81. Geerling GW (2008) Changing rivers: analysing fluvial landscape dynamics using remote sensing. PhD thesis, Centre for Sustainable Management of Resources, Radboud University of Nijmegen, The Netherlands
82. Crocker RI, Maslanik JA, Adler JJ, Palo SE, Herzfeld UC, Emery WJ (2012) A sensor package for ice surface observations using small unmanned aircraft systems. *IEEE Trans Geosci Remote Sens* 50(4):1033–1047
83. Merino L, Caballero F, Martínez-de-Dios JR, Maza I, Ollero A (2012) An unmanned aircraft system for automatic forest fire monitoring and measurement. *J Intell Robot Syst* 65(1): 533–548
84. Martínez-De Dios JR, Ollero A (2006) Automatic detection of windows thermal heat losses in buildings using UAVs. In: 2006 world automation congress, pp 1–6
85. Nagai M, Chen T, Shibasaki R, Kumagai H, Ahmed A (2009) UAV-borne 3-D mapping system by multisensor integration. *IEEE Trans Geosci Remote Sens* 47(3):701–708
86. Lin Y, Hyypä J, Jaakkola A (2011) Mini-UAV-borne LiDAR for fine-scale mapping. *IEEE Geosci Remote Sens Lett* 8(3):426–430



87. Lin Y, Hyypä J, Rosnell T, Jaakkola A, Honkavaara E (2013) Development of a UAV–MMS-collaborative aerial-to-ground remote sensing system—a preparatory field validation. *IEEE J Sel Top Appl Earth Obs Remote Sens* 6(4):1893–1898
88. NORUT. <http://norut.no/>. Accessed 7 Aug 2016
89. Pfeifer N, Glira P, Briese C (2012) Direct georeferencing with onboard navigation components of light-weight UAV platforms. *Int Arch Photogramm Remote Sens Spat Inf Sci XXXIX, Part B7*:487–492
90. Pounds P, Mahony R, Corke P (2010) Modelling and control of a large quadrotor robot. *Control Eng Pract* 18(7):691–699
91. Cesetti A, Frontoni E, Mancini A, Zingaretti P, Longhi S (2009) Vision-based autonomous navigation and landing of an unmanned aerial vehicle using natural landmarks. In: 17th mediterranean conference on control and automation MED’2009, pp 910–915
92. Mittal S, Deb K (2007) Three-dimensional offline path planning for UAVs using multiobjective evolutionary algorithms. In: *IEEE congress on evolutionary computation*, pp 3195–3202
93. Lisein J, Linchant J, Lejeune P, Bouché P, Vermeulen C (2013) Aerial surveys using an unmanned aerial system (UAS): comparison of different methods for estimating the surface area of sampling strips. *J Trop Conserv Sci* 6(4):506–520
94. Whitehead K, Hugenholtz CH (2014) Remote sensing of the environment with small unmanned aircraft systems (UASs), part 1: a review of progress and challenges. *J Unmanned Veh Syst* 2(3):69–85
95. RIEGL USA. Unmanned scanners. <http://products.rieglusa.com/category/all-categories-unmanned-scanners>. Accessed 3 Aug 2016
96. Gu K, Leet J, Alon A, Singh M (2012) E/ME 103 final report. <http://pickar.caltech.edu/e103/papers/Micro%20UAVs.pdf>
97. Calise AJ, Preston D (2008) Swarming/flocking and collision avoidance for mass airdrop of autonomous guided parafoils. *J Guidance, Control Dyn* 31(4):1123–1132
98. Kankare V, Holopainen M, Vastaranta M, Puttonen E, Yu X, Hyypä J, Vaaja M, Hyypä H, Alho P (2013) Individual tree biomass estimation using terrestrial laser scanning. *ISPRS J Photogramm Remote Sens* 75:64–75
99. Vinci A, Brigante R, Todisco F, Mannocchi F, Radicioni F (2015) Measuring rill erosion by laser scanning. *Catena* 124:97–108
100. Maas H-G, Bienert A, Scheller S, Keane E (2008) Automatic forest inventory parameter determination from terrestrial laser scanner data. *Int J Remote Sens* 29(5):1579–1593
101. Côté J-F, Fournier RA, Egli R (2011) An architectural model of trees to estimate forest structural attributes using terrestrial LiDAR. *Environ Model Softw* 26(6):761–777
102. RIEGL USA. Terrestrial Scanners. <http://products.rieglusa.com/category/terrestrial-scanners>. Accessed 3 Aug 2016
103. Kaasalainen S, Jaakkola A, Kaasalainen M, Krooks A, Kukko A (2011) Analysis of incidence angle and distance effects on terrestrial laser scanner intensity: search for correction methods. *Remote Sens* 3(10):2207–2221
104. Mobile Laser Scanning Applications. <http://www.geosignum.nl/index.php/product-services/geosolutions/mobile-laser-scanning>. Accessed 3 Aug 2016
105. Haala N, Peter M, Kremer J, Hunter G (2008) Mobile LiDAR mapping for 3D point cloud collection in urban areas—a performance test. *Int Arch Photogramm Remote Sens Spat Inform Sci* 37:1119–1127
106. RIEGL USA. Mobile scanners. <http://products.rieglusa.com/category/mobile-scanners>. Accessed 3 Aug 2016
107. Trimble MX8. <http://www.trimble.com/Imaging/Trimble-MX8.aspx?tab=Overview>. Accessed 3 Aug 2016
108. James MR, Quinton JN (2014) Ultra-rapid topographic surveying for complex environments: the hand-held mobile laser scanner (HMLS). *Earth Surf Process Land* 39(1):138–142
109. Ryding J, Williams E, Smith MJ, Eichhorn MP (2015) Assessing handheld mobile laser scanners for forest surveys. *Remote Sens* 7(1):1095–1111

110. Bassuk N, Grabosky J, Mucciardi A, Raffel G (2011) Ground-penetrating radar accurately locates tree roots in two soil media under pavement. *Arboric Urban Forest* 37(4):160–166
111. Daniels DJ (2004) Surface-penetrating radar, 2nd edn. The Institute of Electrical Engineers, UK
112. Xie Y, Sha Z, Yu M (2008) Remote sensing imagery in vegetation mapping: a review. *J Plant Ecol* 1(1):9–23
113. Andersen H-E, Strunk J, Temesgen H (2011) Using airborne light detection and ranging as a sampling tool for estimating forest biomass resources in the upper Tanana Valley of interior Alaska. *West J Appl Forest* 26(4):157–164
114. Staahl G, Holm S, Gregoire T, Gobakken T, Næsset E, Nelson R (2011) Model-based inference for biomass estimation in a LiDAR sample survey in Hedmark County, Norway. *Can J Forest Res* 41(1):96–107
115. Reitberger J, Schnörr C, Krzystek P, Stilla U (2009) 3D segmentation of single trees exploiting full waveform LIDAR data. *ISPRS J Photogramm Remote Sens* 64(6):561–574
116. Holopainen M, Mäkinen A, Rasinmäki J, Hyypä J, Hyypä H, Kaartinen H, Viitala R, Vastaranta M, Kangas A (2010) Effect of tree-level airborne laser-scanning measurement accuracy on the timing and expected value of harvest decisions. *Eur J Forest Res* 129(5): 899–907
117. Kaartinen H, Hyypä J, Yu X, Vastaranta M, Hyypä H, Kukko A, Holopainen M, Heipke C, Hirschmugl M, Morsdorf F, Næsset E, Pitkänen J, Popescu S, Solberg S, Wolf BM, Wu J-C (2012) An international comparison of individual tree detection and extraction using airborne laser scanning. *Remote Sens* 4(4):950–974
118. Yao W, Krzystek P, Heurich M (2012) Tree species classification and estimation of stem volume and DBH based on single tree extraction by exploiting airborne full-waveform LiDAR data. *Remote Sens Environ* 123:368–380
119. Vastaranta M, Holopainen M, Yu X, Hyypä J, Mäkinen A, Rasinmäki J, Melkas T, Kaartinen H, Hyypä H (2011) Effects of individual tree detection error sources on forest management planning calculations. *Remote Sens* 3(8):1614–1626
120. Lin Y, Hyypä J, Kukko A, Jaakkola A, Kaartinen H (2012) Tree height growth measurement with single-scan airborne, static terrestrial and mobile laser scanning. *Sensors* 12(9):12798–12813
121. Jaakkola A, Hyypä J, Kukko A, Yu X, Kaartinen H, Lehtomäki M, Lin Y (2010) A low-cost multi-sensoral mobile mapping system and its feasibility for tree measurements. *ISPRS J Photogramm Remote Sens* 65(6):514–522
122. Wallace L, Watson C, Lucieer A (2014) Detecting pruning of individual stems using airborne laser scanning data captured from an unmanned aerial vehicle. *Int J Appl Earth Obs Geoinf* 30:76–85
123. Wallace L, Lucieer A, Watson CS (2014) Evaluating tree detection and segmentation routines on very high resolution UAV LiDAR data. *IEEE Trans Geosci Remote Sens* 52 (12):7619–7628

Handbook on Advances in Remote Sensing and  
Geographic Information Systems  
Paradigms and Applications in Forest Landscape  
Modeling

Favorskaya, M.N.; Jain, L.C.

2017, XIX, 415 p. 109 illus., Hardcover

ISBN: 978-3-319-52306-4